

Raytheon

**SURFACE-CHEMISTRY-DRIVEN TRIBOLOGICAL FUNDAMENTALS
OF DIAMOND AND SIC FOR EXTREME ENVIRONMENT
MEMS APPLICATIONS**

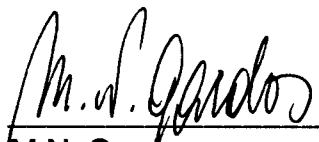
Final Report for the Period 01 August 2000 to 31 December 2000
AFOSR Contract No. FA9620-98-C-0009

31 December 2000

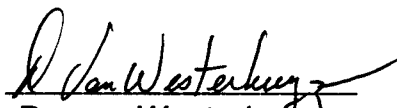
Submitted by:
Engineering Services Center (ESC)
Sensors Engineering (SE)
Raytheon Electronic Systems (RES)
El Segundo, CA 90245

Prepared for:
Lt. Col. Paul C. Trulove, Program Manager

Prepared by:


M.N. Gardos
Sr. Engineering Fellow
RES/SE-ESC

Approved by:


D. van Westerhuyzen
Manager
RES/SE-ESC

DISTRIBUTION STATEMENT A
Approved for Public Release
Distribution Unlimited

DTIC QUALITY INSPECTED 4

20010129 001

REPORT DOCUMENTATION PAGE

AFRL-SR-BL-TR-01-

Public reporting burden for this collection of information is estimated to average 1 hour per response, including gathering and maintaining the data needed, and completing and reviewing the collection of information. Send collection of information, including suggestions for reducing this burden, to Washington Headquarters Services, Davis Highway, Suite 1204, Arlington, VA 22202-4302, and to the Office of Management and Budget, Paperwork I

0041

1. AGENCY USE ONLY (Leave blank)		2. REPORT DATE 31 December 2000		3. REPORT TYPE AND DATES COVERED Final Report, 01 Aug. 2000 - 31 Dec. 2000	
4. TITLE AND SUBTITLE Surface-Chemistry-Driven Tribological Fundamentals of Diamond and SiC for Extreme Environment MEMS Applications				5. FUNDING NUMBERS FA9620-98-C-0009 (Mod. P00003)	
6. AUTHOR(S) Michael N. Gardos					
7. PERFORMING ORGANIZATION NAME(S) AND ADDRESS(ES) Raytheon Electronic Systems Engineering Services Center P.O. Box 902; E1/C182 El Segundo, CA 90245				8. PERFORMING ORGANIZATION REPORT NUMBER	
9. SPONSORING / MONITORING AGENCY NAME(S) AND ADDRESS(ES) Air Force Office of Scientific Research AFOSR/NL 801 No. Randolph St., Room 732 Arlington, VA 22203-7787				10. SPONSORING / MONITORING AGENCY REPORT NUMBER	
11. SUPPLEMENTARY NOTES Lt. Col. Paul C. Trulove, Program Manager					
12a. DISTRIBUTION / AVAILABILITY STATEMENT Distribution Statement A. Approved for public release; distribution is unlimited.				12b. DISTRIBUTION CODE	
13. ABSTRACT (Maximum 200 words) Environmental SEM tribometry of the pressureless-sintered Hexoloy α -SiC ceramics was continued in 0.2 and 3.4 Torr partial pressures of oxygen (PO_2) at room temperature (RT) to 950°C, coupled with after-test SEM photomicrography and AES/XPS surface analyses of the wear scars and the adjacent (unused) surfaces. The results show some correlation in the somewhat improved friction behavior of both the previously tested CERCOM SiC-B in partial pressures of oxygen compared to vacuum, especially when the slower tribo-oxidation kinetics and the surface-oxide-induced reduction in grain pull-out of the boron/carbon-pressed Hexoloy are taken into account. Even in the presence of the thickest lubricating film formed at the 3.4 Torr PO_2 , the COF still did not become reduced below ~0.2 (and the MAX.COF below 0.3). These values are an order-of-magnitude higher than those of the polished PCD. The same observation was made with the SiC-B previously. The wear rate of Hexoloy is only slightly (albeit consistently) less in oxygen than that of the SiC-B, with both in the $10^{-15} m^3/N\cdot m$ range (an order-of-magnitude greater than PCD). Considering the overall tribological behavior of both α -SiC materials, neither is able to serve better than PCD in MEMS moving mechanical assembly applications intended for extreme environments.					
14. SUBJECT TERMS MEMS, poly-XTL α -SiC, friction, wear, SEM tribometry, vacuum, oxygen partial pressures, high temperatures, SEM/AES/XPS analyses, dangling bonds re(de)construction, graphitization, gas-phase lubrication.				15. NUMBER OF PAGES 54	
				16. PRICE CODE	
17. SECURITY CLASSIFICATION OF REPORT Unclassified	18. SECURITY CLASSIFICATION OF THIS PAGE Unclassified	19. SECURITY CLASSIFICATION OF ABSTRACT Unclassified	20. LIMITATION OF ABSTRACT UL		

Table of Contents

	<u>Page</u>
1.0 EXECUTIVE SUMMARY.....	1
2.0 INTRODUCTION.....	1
3.0 EXPERIMENTAL.....	2
3.1 General SEM-Tribometric Test Procedures and Specimens.....	2
3.2 Friction and Wear of Hexoloy in 0.2 and 3.4 Torr Oxygen.....	2
3.3 Wear Scar Surface Analyses.....	4
3.3.1 Quantitative Analyses (All Experiments).....	4
3.3.2 Qualitative Analyses (All Experiments).....	4
3.4 Discussion.....	7
4.0 PRELIMINARY TRIBOMETRIC DATA ON UNCD IN VACUUM.....	8
5.0 CONCLUSIONS	10
6.0 RESEARCH PERSONNEL.....	10
7.0 TRANSITIONS.....	10
8.0 REFERENCES.....	11
APPENDIX: W. Kibbey Stovall, "SiC Tribopin Analysis, Hexoloy Source" RES M&P Dept. Surface Analysis Laboratory Report, 9/20/00.	

Foreword

The main objective of this three-year AFOSR/NL program extension is to determine the surface chemistry-driven tribological fundamentals of polycrystalline diamond (PCD) and α -SiC as bearing materials for extreme-environment microelectromechanical systems moving mechanical assemblies (MEMS-MMAs). The most harmful extreme environmental effect is defined here as tribochemical wear suffered in various partial pressures of molecular oxygen, in a wide temperature range represented by thermal ramping from room temperature to 950 °C and back to room temperature. The focus is on (a) understanding the tribochemical wear mechanisms increasing or reducing the friction and wear of PCD and α -SiC via volatile (PCD \rightarrow CO and CO₂) or glassy (SiC \rightarrow SiO_x) oxide formation, as counterbalanced by stable Si-O or C-O surface moieties acting as passivating adsorbates for dangling bonds. The title of the program is "Surface-Chemistry-Driven Tribological Fundamentals of Diamond and SiC for Extreme Environment MEMS Applications", with a start date of 15 November 1997. This Final Report covers a portion of the work done during the third year of the program extension, between 01 August 2000 and 31 December 2000.

List of Tables

- Table 1. Wide temperature range wear rates of polished and variously cleaned SiC-B sliding against itself in vacuum and 0.2 and 3.4 Torr P_{O_2} .
- Table 2. Wide temperature range wear rates of polished and variously cleaned Hexoloy SiC sliding against itself in vacuum and 0.2 and 3.4 Torr P_{O_2} .
- Table 3. AES/XPS-measured atomic concentration of the hexane+HF-washed and 0.2 Torr O_2 -tested Hexoloy SiC flat off and on the wear tracks.
- Table 4. AES/XPS-measured atomic concentration of the hexane+HF-washed and 3.4 Torr O_2 -tested Hexoloy SiC tribopin.

List of Figures

- Figure 1. COF of hexane-washed and hexane+HF-washed Hexoloy SiC in vacuum, 0.2 Torr and 3.4 Torr P_{O_2} .
- Figure 2. MAX.COF of hexane-washed and hexane+HF-washed Hexoloy SiC in vacuum, 0.2 Torr and 3.4 Torr P_{O_2} .
- Figure 3. Normal incidence SEM photomicrographs of hexane+HF-washed Hexoloy SiC pin wear scars, as-tested in 0.2 and 3.4 Torr P_{O_2} ; double-headed arrows indicate direction of sliding.
- Figure 4. SEM photomicrographs of hexane+HF-washed Hexoloy SiC pin wear scar surrounded by wear debris, as-tested in 3.4 Torr P_{O_2} ; photo taken on-centerline (left) and slightly off-centerline (right).
- Figure 5. Shallow angle SEM photomicrographs of the hexane+HF-washed Hexoloy SiC pin wear scar edge, as-tested in 0.2 Torr and 3.4 Torr P_{O_2} , showing the scar texture and wear debris morphologies, at various magnifications. Double-headed arrows indicate direction of sliding.
- Figure 6. Normal incidence SEM photomicrographs of hexane+HF-washed Hexoloy SiC flat wear scars, as-tested in 0.2 Torr P_{O_2} , showing early scar texture and wear debris morphologies; double-headed arrows indicate direction of sliding.
- Figure 7. Normal incidence SEM photomicrographs of hexane+HF-washed Hexoloy SiC flat wear scars, as-tested in 0.2 Torr P_{O_2} , showing mature scar textures and wear debris morphologies; double-headed arrows indicate direction of sliding.
- Figure 8. Normal incidence SEM photomicrographs of hexane+HF-washed Hexoloy SiC flat wear scars, as-tested in 3.4 Torr P_{O_2} , showing early scar textures and wear debris morphologies; double-headed arrows indicate direction of sliding.
- Figure 9. Normal incidence SEM photomicrographs of hexane+HF-washed Hexoloy SiC flat wear scars, as-tested in 3.4 Torr P_{O_2} , showing mature scar textures and wear debris morphologies; double-headed arrows indicate direction of sliding.

- Figure 10. Similarities in the "rolling pin" wear debris appearance of Hexoloy SiC and CERCOM SiC-B.
- Figure 11. Shallow angle SAM photomicrographs of the hexane+HF-washed Hexoloy SiC pin wear scar, as-tested in 0.2 Torr and 3.4 Torr PO_2 (arrows indicate analytical sites); various magnifications (also see Tables 3 and 4).
- Figure 12. Wide-scan survey XPS spectra of the hexane+HF-washed and 0.2 Torr PO_2 -tested Hexoloy SiC pin tip wear scar, in the as-tested+Ar-sputtered (top) and wiped+Ar-sputtered (bottom) conditions; also see Table 3). Ar-sputtering removed 1 nm in each case.
- Figure 13. Multiplexed XPS spectra of the hexane+HF-washed and 0.2 Torr PO_2 -tested Hexoloy SiC pin tip wear scar, in the as-tested+Ar-sputtered (top) and wiped+Ar-sputtered (bottom) conditions; also see Table 3). Ar-sputtering removed 1 nm in each case.
- Figure 14. Deconvoluted Si, C and O spectral peaks of hexane+HF-washed and 0.2 Torr PO_2 -tested Hexoloy SiC pin tip wear scar, in the as-tested+Ar-sputtered condition (also see Table 3). Ar-sputtering removed 1 nm. Peak assignments: Si2p peaks: 100.0 eV = carbidic, 102.2 eV = Si-O, silicates; C1s peaks: 282.7 carbidic, 284.6 eV = graphitic, 286.7 = C-O, C=O; O1s peak: 532.0 eV = O-Si, organic carbonyls.
- Figure 15. Deconvoluted Si, C and O spectral peaks of hexane+HF-washed and 0.2 Torr PO_2 -tested Hexoloy SiC pin tip wear scar, in the wiped+Ar-sputtered condition (also see Table 3). Ar-sputtering removed 1 nm. Peak assignments: Si2p peaks: 100.0 eV = carbidic, 102.2 eV = Si-O, silicates; C1s peaks: 282.7 carbidic, 284.6 eV = graphitic, 286.7 = C-O, C=O; O1s peak: 532.0 eV = O-Si, organic carbonyls.
- Figure 16. Wide-scan survey XPS spectra of the hexane+HF-washed and 3.4 Torr PO_2 -tested Hexoloy SiC pin tip wear scar, in the as-tested+Ar-sputtered (top) and wiped+Ar-sputtered (bottom) conditions; also see Table 4). Ar-sputtering removed 0.5 nm in each case.
- Figure 17. Multiplexed XPS spectra of the hexane+HF-washed and 3.4 Torr PO_2 -tested Hexoloy SiC pin tip wear scar, in the as-tested+Ar-sputtered (top) and wiped+Ar-sputtered (bottom) conditions; also see Table 4). Ar-sputtering removed 0.5 nm in each case.
- Figure 18. Deconvoluted Si, C and O spectral peaks of hexane+HF-washed and 3.4 Torr PO_2 -tested Hexoloy SiC pin tip wear scar, in the wiped+Ar-sputtered condition (also see Table 4). Ar-sputtering removed 0.5 nm. Peak assignments: Si2p peaks: 100.0 eV = carbidic, 102.2 eV = Si-O, silicates, 105.8 eV = anomalously high value; C1s peaks: 282.7 carbidic, 284.6 eV = graphitic, 286.7 = C-O, C=O; O1s peaks : 532.0 eV = O-Si, organic carbonyls, 535.2 eV = anomalously high value.
- Figure 19. Improved deconvolution of the C1s spectral peak of hexane+HF-washed and 3.4 Torr PO_2 -tested Hexoloy SiC pin tip wear scar, in the as-tested+Ar-sputtered condition. Ar-sputtering removed 0.5 nm. The dotted error function is significantly smoothed by incorporating the third peak.

- Figure 20. Deconvoluted Si, C and O spectral peaks of hexane+HF-washed and 3.4 Torr PO_2 -tested Hexoloy SiC pin tip wear scar, in the wiped+Ar-sputtered condition (also see Table 4). Ar-sputtering removed 1 nm. Peak assignments: $\text{Si}2p$ peaks: 100.0 eV = carbidic, 102.2 eV = Si-O, silicates; $\text{C}1s$ peaks: 282.7 eV = carbidic, 284.6 eV = graphitic, 286.7 = C-O, C=O; $\text{O}1s$ peaks : 532.0 eV = O-Si, organic carbonyls.
- Figure 21. Auger spectra of the oxide ($\sqrt{3} \times \sqrt{3}$) $R30^\circ$ structures on both crystal orientations [(a): $\text{SiC}(0001)$; (b) $\text{SiC}(000\bar{1})$]. Both spectra display an oxygen peak as well as oxygen-related features in the $\text{Si}_{L_{VV}}$ peak (shown with enlarged energy scale in the inset). These features vanish when heating the sample at 1050°C [e.g., (c): $(000\bar{1})$ surface]; from [2].
- Figure 22. Friction (f) and wear rate (k_w) of a sintered SiC sliding against itself in air, at various speeds and temperatures (pin-on-disc test configuration); from [3].
- Figure 23. Pull-off force (adhesion) as a function of temperature for SiC {0001} flat surfaces in contact with sintered polycrystalline SiC pins in ultrahigh vacuum; from [4].
- Figure 24. Shallow angle SEM photo of the $\sim 2 \mu\text{m}$ -thick UNCD-coated CERCOM SiC-B tribopin positioned in its graphite fixture, right after removal from the deposition chamber.
- Figure 25. COF and MAX.COF of the UNCD in vacuum. Note graphite-like (high friction) behavior in vacuum, and favorable (equally graphite-like) friction response to various partial pressures of 50% R.H. air admitted into the chamber.
- Figure 26. Size and appearance of the worn UNCD on the pin tip scar. Numbers indicate sites of forthcoming AEX/XPS/micro-Raman examinations.

1.0 EXECUTIVE SUMMARY

Environmental SEM tribometry of the pressureless-sintered Hexoloy α -SiC ceramic was continued in 0.2 and 3.4 Torr partial pressures of oxygen (P_{O_2}) at room temperature to 950°C, coupled with after-test SEM photomicrography and AES/XPS surface analyses of the wear scars and the adjacent (unused) surfaces. It was previously shown that the silicon and poly-crystalline diamond (PCD)-like behavior of CERCOM's pressure-assisted-densified (PAD) SiC-B α -SiC *in vacuum* is not followed by the consistently higher friction Hexoloy. The root cause appears to be the continuous intergranular failure (pull-out) of the poorly bonded Hexoloy micrograins sheared on the sliding surfaces under high friction forces.

As demonstrated in this report, there is some correlation in the somewhat improved friction behavior of both materials in partial pressures of oxygen compared to vacuum, especially when the slower tribo-oxidation kinetics and the surface-oxide-induced reduction in grain pull-out of the boron/carbon-pressed Hexoloy are taken into account. However, the wear rate of Hexoloy is only slightly (albeit consistently) less in oxygen than that of the SiC-B. Considering the overall tribological behavior of both α -SiC materials, neither is able to serve better than PCD in MEMS moving mechanical assembly applications intended for extreme environments.

In preparation for the next 3-year grant period concentrating on quantifying the tribo-oxidative kinetics and top temperature/ P_{O_2} limits of both polished PCD and the Argonne ultra-nanocrystalline diamond (UNCD), a few preliminary vacuum tests were performed on $\sim 2\ \mu\text{m}$ UNCD deposited on SiC-B pin/flat specimens. The data indicate that the UNCD exhibits consistently high friction, graphite-like (and definitely not PCD-like) behavior, with a wear rate of $1.12 \times 10^{-14}\ \text{m}^3/\text{N}\cdot\text{m}$, 4 to 5-times higher than the equivalent values of either α -SiC material in vacuum. UNCD needs gas-phase lubrication considerably more than polished PCD.

2.0 INTRODUCTION

The poor intergranular bond strength of the Hexoloy SiC (an undesirable trait, leading to high friction and wear in vacuum, see [1]) is juxtaposed in this report with its friction/wear-mitigating, slower oxidation kinetics. A lower rate of oxidation is attributed to its boron-carbon-type sintering aid, which should (and did) reduce the tribo-oxidative wear somewhat, compared to that of SiC-B. Therefore, the main object of concern during the present grant period was to find out the differences (if any) in the tribo-oxidative behavior and surface chemistry of the highly consolidated (but faster oxidative kinetics) SiC-B versus the behavior of the more porous (weaker) but slower-oxidizing Hexoloy.

3.0 EXPERIMENTAL

3.1 General SEM-Tribometric Test Procedures and Specimens

The SEM tribometer, as well as the procedures for preparing and testing silicon, silicon carbide and PCD test specimens are adequately described in [1] and the related papers referenced therein. It suffices to note that two tests are normally run in the same flat track in a specific environment for $2 \times 2000 = 4000$ cycles, then the used pin is made to slide against a new track (which has been heated but not rubbed in the same environment) for another 4000 cycles.

3.2 Friction and Wear of Hexoloy in 0.2 and 3.4 Torr P_{O_2}

The examination of the COF (Figure 1) and MAX.COF (Figure 2) data generated with the hexane+HF-cleaned specimens sliding in vacuum versus P_{O_2} indicates that oxygen (i.e., an oxide surface layer) acts as a pseudo-lubricant, but only at the higher partial pressure. The appearance of the "rabbit ear" signature during the fourth test in 0.2 Torr oxygen (generated after static heating of the used portion twice, followed by dynamic oxidation of the wear scar once before the last test) seemed to indicate some healing (adhesive-gluing) effect of an extremely thin (and possibly incomplete) oxide layer on the surface or in the grain boundaries. The severely reduced grain pull-out apparently permitted the formation and reconstruction of the dangling bonds. They could form where the volatile SiO_x species were torn from the surface, leaving unsaturated bonds behind [1]. A parallel exists with oxidizing diamond, during the generation of the volatile CO and CO_2 .

This surface effect appears to be significant in influencing the shape of the friction curves, because SiO and SiO_x (formed in small P_{O_2}) are indeed volatile, leaving progressively less (but still observable) surface oxide at gradually smaller P_{O_2} . As previously reported in [1], experiments examining the effects of the above reactions on the strength of the Hexoloy SiC were performed in flowing Ar gas at 1400°C , containing various partial pressures of pure oxygen. *Where the P_{O_2} was higher than 3×10^{-5} MPa (0.22 Torr), SiO_2 formed on the surface (i.e., passive oxidation occurred) and the strength of the samples was not significantly affected. Where the P_{O_2} was lower than 2×10^{-5} MPa (0.15 Torr), active oxidation caused material loss, decreasing the weight and the strength of the samples. Active oxidation caused severe surface degradation such as grain boundary attack and the formation of large pits responsible for the degradation of strength. The surface analytical results given in the previous AFOSR report [1] and Section 3.3 of the present report confirm this phenomenon.*

The friction data in 3.4 Torr (Figures 1 and 2) can be explained by considering an oxide formation versus removal balance. The traces begin with the same "rabbit ear"-type trend of the last 0.2 Torr test. This can happen only if an extremely thin oxide layer provides the lowest friction at room temperature without being completely removed by the sliding action, but volatilizes at high temperatures. The evaporating SiO generates dangling surface bonds, which then attempt to re(de)construct. On cooling, the re-established (but still extremely thin) oxide reduces the friction. On repeated heating the oxide becomes gradually thicker (with a possible change from SiO_x to SiO_{2-x}), lowering the friction on cooling. This trend resembles that of oxidizing SiC-B and oxidizing diamond [1]. As before with SiC-B, even in the presence of the thickest lubricating film formed, the COF is still not reduced below ~ 0.2 (or the MAX.COF below 0.3).

The wear rates (\mathcal{W}) in Table 1 were calculated per Figure 5. The values, compared with those of SiC-B from [1] (Table 2) indicate that the tribooxidative kinetics of the two materials are very close, with a somewhat lower rate for the more oxidation resistant Hexoloy, its porosity notwithstanding. The \mathcal{W} are about an order of magnitude greater than those of polished PCD. As also shown in Figure 5, the wear scar is textured and there is some frosting, along with the evidence of the ubiquitous porosity of the pressureless-sintered Hexoloy. However, the scars associated with both partial pressures of oxygen are far smoother than those observed after the vacuum tests in [1]. The partially oxidized flat scars and the characteristic debris shapes described in Figures 6 through 10 show the following:

1. The scars on the flats have smooth and rough areas. However, they are generally smoother with less grain pull-out than the more highly stressed pin scars. Note that more oxide can be formed than removed on/off the flat versus what occurred on/off the pin tip. The typical porosity of the material is clearly depicted.
2. The wear debris has two characteristic shapes, i.e., consolidated platelets and rod-like "rolling pins", at both partial pressures. However, there is a far greater prevalence of the micro-rolls at 3.4 Torr. The photo in Figure 10 indicates that the formation mechanism of these rolling pins on both SiC-B [1] and Hexoloy are identical: where the oxidation kinetics are fast enough to form enough viscous SiO_{2-x} on the surface to generate tiny rolls during sliding, they can form in greater numbers. Clearly, their formation in 0.2 Torr is severely retarded, because unevaporated (residual) SiO_x on the surface (if any at all, see the forthcoming surface-analytical results) is hard and brittle. Note that the larger number of rolls at 3.4 Torr coincides with the more effectively reduced friction at that pressure (see Figures 1 and 2), as previously discussed with SiC-B in [1].

3.3 Pin Tip Wear Scar Surface Analyses

3.3.1 Quantitative (AES) Analyses (Figure 11; Tables 3 and 4; the Appendix)

The bright- and dark-contrasted areas observed in the SEM images in Figure 5 were not seen in the SAM images in Figure 11. The analyses of the various sites indicated in the latter illustration yielded data similar to the AES/XPS of the SiC-B presented previously in [1]:

1. The near-absence of Si on the wear scar surface after the 0.2 Torr tests is real. Even though the smooth area (after the removal of a 5Å surface layer by sputtering) yielded a numerical value of 14 at.% for Si (see AES survey results in Table 3), this amount is at the noise level of the spectrum. The rough area shows just carbon, with oxygen appearing only in the subsurface in extremely small quantities. Even the unrubbed area next to the scar contained only some oxidized surface carbon - - no Si. The stoichiometry of the debris was that of SiO (an Si/O at.% ratio of 1), with a great deal of surface carbon.
2. While the 0.2 Torr-tested pin showed the least surface oxygen and silicon, the 3.4 Torr-tested pin tip scar showed 10 at.% on the low relief areas (still an extremely low value) and as much as 30 at.% at the high relief areas shown in Figure 5. In these areas both the Si/O and C/O ratios become reduced to 75% of the equivalent ratios of the low surface relief areas. Note that the high relief plateaus essentially represents the real area of contact in the scar - - tribooxidative kinetics of the most severely rubbed microcontacts are faster (generating more oxide) than the more static oxidation of the less vigorously rubbed micro-areas (generating less oxide). The same trend for the unworn areas was not as pronounced.
3. The fine, granular wear debris exhibited an increasing oxygen content with a higher PO_2 .

3.3.2 Qualitative (XPS) Analyses (Figures 11, 12 through 20; Tables 3 and 4; the Appendix)

As before with the analyses of the SiC-B in [1], *quantitative* XPS analyses of the wear scars could not be done, because the scar and its features were smaller than the smallest XPS aperture available (200 µm). The spectra presented in Figures 12 through 20 include unworn areas and debris before and after wiping the tips. As a consequence, the XPS spectra represent area-weighted averages of the surfaces analyzed within a 100 µm radius from the center of the wear scar, with a portion of the unrubbed surface included. This artifact also prevented using the integrated areas of the deconvoluted peaks as absolute measures of the scar's chemical

composition, although relative comparisons of the "as-tested" and "wiped" areas can be made. Nevertheless, the peak energies are still meaningful. For the peak fits reported here, a minimum number of peaks were used with a requirement that the FWHM of each be less than ~2.5 eV.

As further discussed in the Appendix, the chemical states are assigned by correlating the peak energies of the deconvoluted C1s, O1s, and Si2p emissions with reported energies from known samples:

1. In the case of the C1s emission, the XPS multiplexes for the three samples show the element to be in three binding energy states, averaging 283.6 eV, 284.4 eV, and 286.7 eV. The lowest value best corresponds with reference values for carbidic carbon (280.7 to 285.0 eV) and occurred for all pins. The middle value is in the range of graphitic (284.2 to 285.0 eV) carbon, strongly appearing in the 0.2 Torr-tested sample only. The high-energy value was seen in both pins and best matches with the expected energies of carbon atoms singly or doubly bonded to oxygen (286.0 to 288.0 eV). This would include alcohol, ether, ketone, and aldehyde functionalities, but exclude carboxyls and carbonates.
2. The Si2p emissions showed two dominant components: a low energy peak at 100.1 eV and a higher peak at 102.3 eV, along with an aberrant 105.8 eV peak for the 3.4 Torr-tested pin. The low energy peak falls at the low end of the reported values for carbides (99.9-100.9 eV), while the higher peak overlaps best with silicates (102.0-103.0 eV). The reported range for SiO₂ does not begin until binding energies in excess of 103.2 eV are reached, but no reported Si valence is in excess of 104.5 eV. The unusually high energy peak may have originated from oxide surface charging or from the presence of silicon oxycarbides, as discussed later in this report.
3. The O1s emissions occurred only as single peaks for the vacuum and 0.2 Torr tests, but the 3.4 Torr test also yielded a majority component at a higher energy. The low energy peaks were centered around 532.0 eV (which is lower than the values typically reported for SiO₂ = 532.5-534.3 eV, but is similar to values seen for organic carbonyls such as *p*-benzoquinone and benzamide. The anomalously high energy (charging?) peak on the 3.4 Torr-tested pin appeared at 535.2 eV, above the reported valence of any oxygen species.

When interpreting the photoelectron data, note that they represent the area-weighted averages of the whole tip surfaces, which included the wear scar, wear debris and a portion of the unworn tip. Furthermore, an effort was made only to use the minimum number of peaks required to produce a good mathematical fit for the data. However, because it was felt that for the 0.2 Torr

C1s test data this did not produce realistic results, an additional peak was used in Figure 19 to reduce the fitting error and produce values more in line with previous interpretations.

Accordingly, the surface of the 3.4 Torr-tested pin showed (a) primarily carbidic carbon with a lesser amount of oxygenated carbon, (b) carbidic silicon, and oxygenated silicon, and (c) a single oxygen value appropriate to both, with the exception of the additional, anomalously high valence oxygen and silicon peaks attributed to localized regions of silica. As previously mentioned, these regions (most likely in the wear debris judging by the high O/Si ratio seen there by AES) charged slightly and therefore shifted their peaks, or there are silicon oxycarbide species present, as before in [1] (Figure 18). There was no graphitic C1s found on the 3.4 Torr-tested pins. Sufficiently good fits to the data were obtained using just the carbidic and oxygenated energy peaks. While it could have been possible to add a graphitic peak and obtain a good fit, the contribution to the overall peak shape from this valence would have been small. It is known and was mentioned in [1] that there is greater etching of the carbon-graphitic phase in higher partial pressures of oxygen, consistent with the present finding.

The 0.2 Torr-tested pin's elemental AES analyses and XPS results suggested that (a) its surface carbon was primarily graphitic with smaller amounts of carbidic and oxygenated carbon, and (b) its silicon was both carbidic and oxygenated, with an oxygen energy peak value appropriate to both.

Multiplexed XPS data were also taken from the tips before and after removal of the loose debris by firmly wiping the tips with isopropyl alcohol-soaked "Kaydry" laboratory tissues. Differences between the before/after results should, therefore, come from the removal of the debris. After cleaning, both tips showed a decrease in silicon content, but only a slight increase in carbon content. Since no additional Ar-sputter-cleaning was done after wiping and there might be a slight chance of possible deposition of organic deposits originating from the solvent and the wipe, removal from UHV and subsequent wiping and reintroduction of the sample into UHV without sputtering thereafter was expected to somewhat increase the adventitious carbon content of the surfaces. The carbon content of the 0.2 Torr-tested pin indeed increased slightly, while it decreased for the 3.4 Torr-tested (oxygen-etched) scar.

The 0.2 Torr-tested pin had much less debris than the 3.4 Torr equivalent. This suggests that the drop in both silicon and oxygen content at the higher PO_2 was caused by the removal of the debris exhibiting primarily that composition. The loss of Si from the wiped 0.2 Torr pin tip indicates that the debris there (just like on the vacuum-tested pin tip) was primarily Si and silicon plus carbon in content. The multiplexes for the unwiped 3.4 Torr pin were essentially same as for

the wiped tip, but with the additional, anomalously high-valence oxygen and silicon peaks (compare Figure 17 with Figures 18 and 20). As before, these high binding energy peaks are either attributed to localized regions of non-conductive (charging) SiO_x and SiO_{2-x} or are representative of the silicon oxycarbide species previously discussed thoroughly in [1]. Since these peaks disappeared after wiping, these regions are in the debris.

3.4 Discussion

It was found both in [1] with SiC-B and Hexoloy that maintenance of the lowest $\text{COF} \cong 0.2$ and $\text{MAX.COF} \cong 0.4$ in 3.4 Torr PO_2 is predicated upon the formation versus removal balance for the lubricious SiO_{2-x} (with x close to 2) and silicon oxycarbide surface layer under the particular SEM-tribometric conditions used, and (b) volatile removal of the carbon-graphite phase through oxygen-carbon and hydroxyl-carbon reaction (carbon-etching) pathways. The SiO_x or SiO_{2-x} surface layer, which forms on statically oxidized SiC, tends to disappear after heating to 1050°C due to volatilization of SiO (see Figure 21 taken from [2]).

Other information from the literature confirms (a) the formation of viscous surface oxides on sintered α -SiC, providing some reduction in friction at low sliding speeds and high temperatures, in air (but not at low temperatures at any speed), see Figure 22 [3]. As shown in that illustration, the COF decreases from 0.8 to 0.6 with increasing speed, while the wear coefficient increases in the opposite direction. At higher temperatures, the COF shows a larger scatter between 0.2 and 0.8 even for constant test conditions. This is also valid for the wear coefficient at 800°C and 1000°C . The 400 to 800°C , low-speed wear coefficients under unidirectional pin-on-disc sliding in air are in the $10^{-14} \text{ m}^3/\text{N}\cdot\text{m}$ range. This regime is about an order of magnitude higher than the SEM-tribometric (oscillatory) wear coefficients under thermal ramping to 850°C at ultra-low speed oscillatory conditions, in 3.4 Torr oxygen (Table 2).

Small-spot XPS analysis in [3] revealed that the wear scars which yielded low friction and wear were covered by a thin, tribochemically formed oxide layer. Higher COF and wear coefficients were correlated with much thicker oxide layers.

The appearance of the first, double-lobed "rabbit ear" friction signature of SiC was manifested by SiC-B in [1], and to some extent with Hexoloy in Figures 1 and 2. Superposition of the equivalent silicon and PCD friction signatures in [1] indicated that this double frictional increase on heating could be attributed to the different bond strengths of Si-H and C-H present on the SiC surfaces, and the generation of high friction dangling bonds in two major thermal regimes

associated with these broken bonds on heating. For the first time, independent confirmation of this double friction lobe on a similar thermal upramp in UHV can be found in [4], as shown in Figure 23. However, Miyoshi (the author) did not explain the origin of this friction artifact.

4.0 PRELIMINARY TRIBOMETRIC DATA ON UNCD IN VACUUM

The AFOSR-funded Raytheon studies to date have indicated that PCD performs significantly better than Si or α -SiC at room and high temperature in an oxidizing atmosphere, for extreme environment MEMS applications. However, as the hardest-known and most chemically inert material, diamond is difficult to process. Furthermore, conventional vapor phase deposition methods produce PCD coatings with rough surface morphologies that are unsuitable for MEMS applications. A few years ago, a new microwave plasma deposition technique was developed at Argonne National Laboratory (ANL), producing phase-pure ultrananocrystalline diamond (UNCD) coatings with unique mechanical, tribological, surface finish (no polishing required after deposition) and thermal properties that are ideally suited for both static and dynamic MEMS applications. In addition, a selective UNCD deposition and etching technique has also been developed to produce integrated MEMS structures (static and dynamic) without any need for hand assembly.

The UNCD process for growth of phase-pure nanocrystalline diamond utilizes microwave plasma-enhanced chemical vapor deposition using Ar-CH₄ or Ar-C₆₀ plasmas with very low hydrogen levels [5]. The growth proceeds via incorporation of gas-phase carbon dimers directly into the diamond lattice. For very small grain size (≤ 5 nm), the surface free energy contribution to the energy of formation is sufficient to make diamond the thermodynamically stable phase of carbon. Because of the near-absence of atomic hydrogen in the UNCD growth process, little gasification of nascent diamond grains occurs. This results in an extremely high effective renucleation rate that yields nanocrystalline (5 to 10 nm grain size) phase pure (sp³) diamond coatings with rms roughness of 20 to 50 nm (~20 to 50 times less than conventional CVD diamond films), even for thick films. Measurements indicated that only 2 to 3% sp²-bonding is found in the coating, and about 50 to 80% of that reside at the grain boundaries. This effectively means that the grain boundary surfaces are essentially reconstructed, containing no carbon-graphitic material. Because of the large grain boundary-to-nanograin volume ratio, the UNCD would have a considerable amount of sp² bonding exposed on the sliding surfaces. This would clearly affect the friction signatures.

Tribological investigation of this coating, comparing its performance to the more conventional, polished-microcrystalline PCD in various atmospheric environments and temperatures has been made a part of a three-year Raytheon study, commencing in CY 2001. In

preparation for this upcoming work, the last task of running polished PCD in only 10 liters of available tagged oxygen at 3.4 Torr, at elevated temperatures until the gas ran out, was replaced by 4 ea. vacuum tribotests of the UNCD.

A SiB tribopin and flat couple was pretreated for enhanced nucleation by ultrasonic seeding (0.1 μm diamond powder in methanol, for 15 min.), followed by microwave plasma coating with $\sim 2\mu\text{m}$ UNCD. During the run, the pin was positioned, side-by-side with the flat and at the same level on the ANL deposition chamber's substrate table, in a close-fitting hole drilled into a graphite support block. Only the tip protruded during the deposition process (Figure 24). The Raman spectra of the film indicated a good deposition run.

This specimen combination was subjected to 4 ea. conventionally thermal-ramped (to 950°C) SEM-tribometric experiments at $\sim 1 \times 10^{-5}$ Torr. First, two tests were run in one flat scar, followed by moving the flat under the used pin to a fresh (but previously twice-heated) flat area for two more tests in the new wear scar, without breaking vacuum.

The data in Figure 25 indicate that the UNCD behaves more like graphite than the PCD examined previously under identical conditions. The rapid drop in friction on admitting atmospheric humidity-containing air into the chamber at various partial pressures is an especially graphite-like behavior. The SEM photomicrographs of the wear scar, taken at a 45° angle, indicate considerable wear compared to PCD or even the two $\alpha\text{-SiC}$ compounds recently tested. *The UNCD wear rate was calculated to be $1.12 \times 10^{-14} \text{ m}^3/\text{N}\cdot\text{m}$, about 4 to 5 times higher than $\alpha\text{-SiC}$ (see Tables 1 and 2) and about two orders-of-magnitude higher than polished PCD. The data indicate an extreme need for gas-phase lubrication of UNCD with water vapor or other suitable gases.*

The various sites indicated in Figure 26 by the numbered arrows are now undergoing AES, micro-Raman and possibly EELS analysis at Raytheon and Argonne to look for any measurable graphitization of the wear scar surface. The results will be reported in the first Progress Report of the new grant period.

5.0 CONCLUSIONS

Environmental SEM tribometry of the pressureless-sintered Hexoloy α -SiC ceramics was continued in 0.2 and 3.4 Torr partial pressures of oxygen (P_{O_2}) at room temperature (RT) to 950°C, coupled with after-test SEM photomicrography and AES/XPS surface analyses of the wear scars and the adjacent (unused) surfaces.

The results show some correlation in the somewhat improved friction behavior of both the previously tested CERCOM SiC-B in partial pressures of oxygen compared to vacuum, especially when the slower tribo-oxidation kinetics and the surface-oxide-induced reduction in grain pull-out of the boron/carbon-pressed Hexoloy are taken into account. Even in the presence of the thickest lubricating film formed at the 3.4 Torr P_{O_2} , the COF still did not become reduced below ~ 0.2 (and the MAX.COF below 0.3). The same observation was made with the SiC-B previously. The wear rate of Hexoloy is only slightly (albeit consistently) less in oxygen than that of the SiC-B, with both being in the $10^{-15} \text{ m}^3/\text{N}\cdot\text{m}$ regime (an order-of-magnitude greater than PCD). Considering the overall tribological behavior of both α -SiC materials, neither is able to serve better than PCD in MEMS moving mechanical assembly applications intended for extreme environments.

6.0 RESEARCH PERSONNEL

The work has been performed by members of the RES tribology team directed by Dr. Mike Gardos as the Program Manager/Principal Investigator, e-mail: mngardos@west.raytheon.com; Ph.: (310) 647-4357 and FAX: (310) 647-4378, with administrative support from Mr. Mike Lohnes Contracts Administrator. Messrs. Lindon Melton, Bruce Buller, Geoff Nash and Drs. Kurt Ketola and Kibbey Stovall performed the tribological and analytical characterization.

7.0 TRANSITIONS

The PCD and α -SiC results have been disseminated in the following papers:

- M.N. Gardos, "Determining the Nanoscale Friction and Wear Behavior of Si, SiC and Diamond by Microscale Environmental Tribology," invited paper presented at the NATO-ASI Course on "Fundamentals of Tribology and Bridging the Gap Between Macro- and Micro/Nanoscale Tribology," Aug. 13-25, 2000, Keszthely, Hungary, (Ed. B. Bhushan), Kluwer (in press).

- M.N. Gardos, "Environmental Tribology," invited paper presented at the 27th Leeds-Lyon Symp. on Tribology, Sept. 5-8, 2000, INSA, Lyon, France, Elsevier (in press).

In addition, there are two main transitions in the form of upcoming DARPA proposals. Both are in conjunction with Argonne National Laboratory, involving the use of their UNCD in dynamic MEMS applications. The contact at ANL is Dr. Orlando Auciello (the Proposal Manager in each case, tel.: (630) 252-1685, fax: (630) 252-4798, e-mail: auciello@anl.gov).

The first transition is our reply to Bill Tang's recent BAA 01-09 ("Micro-Power Generation"). The proposed work involves the design and evaluation of air-driven pinwheel-type AC/DC electrical generators fabricated from UNCD, used as mitochondrial power sources for MEMS aerodynamic control actuators and other MEMS sensors/actuators operated in air streams ripe for harvesting. The team includes ANL, Sandia and Raytheon.

The second transition is a full proposal to DARPA/DSO's Palm Power BAA 01-18 due on Feb. 1, 2001. Our Argonne/Stanford/Creare/Raytheon team intends to demonstrate a mesoturbine operating at ~ 400,000 rpm with a cycle thermal efficiency of ~33% and 50 W of power, enabled by UNCD-coated MEMS components. Note that no White Papers are required before that date. This proposal, as well as the preproposal described above, are made possible by the previous AFOSR research conducted by the present Raytheon tribo-team.

8.0 REFERENCES

1. M.N. Gardos, "Surface-chemistry-driven Tribological Fundamentals of Diamond and SiC for Extreme Environment MEMS Applications," Progress Report for the Period 01 August 199 to 31 July 2000, AFOSR Contract No. FA9620-98-C-0009, Raytheon Systems Company, El Segundo, CA 90245, 30 August 2000.
2. J. Bernhardt, J. Schardt, U. Starke and K. Heinz, "Epitaxially Ideal Oxide-Semiconductor Interfaces: Silicate Adlayers on Hexagonal (0001) and (0001) SiC Surfaces," *Appl. Phys. Lett.*, 74, pp. 1084-1086 (1999).
3. K.-H. Habig and M. Woydt, "Sliding Friction and Wear of Al_2O_3 , ZrO_2 , SiC and Si_3N_4 ," in *Proc. 5th Int. Congress on Tribology*, Espoo, Finland, 3, pp. 106-113 (1989); also see K.-H. Habig, "Tribologisches Verhalten von Ingenieur-Keramik," *Ingenieur-Werkstoffe*, 1, pp. 78-83 (1989).
4. K. Miyoshi, "Considerations in Vacuum Tribology (Adhesion, Friction, Wear and Solid Lubrication in Vacuum)," *Tribol. Int.*, 32, pp. 605-616 (1999).
5. T. D. Corrigan, O. Auciello, A. R. Krauss, D. M. Gruen and R. P. H. Chang, "Integration of Ultrananocrystalline Diamond Films on Glass Substrates for Field Emission Displays", *Mater. Res. Soc. Symp. Proc.*, Vol. 593, pp. 233-236 (2000).

Table 1. Wide temperature range wear rates of polished and chemically cleaned Hexoloy SiC sliding against itself in vacuum and 0.2 and 3.4 Torr P_{O_2} .

Atmosphere	Specimen Cleaning Method	Stress (MPa)		Pin Wear Rate ($m^3/N \cdot m$)	No. of cycles
		Start	End		
$\sim 1 \times 10^{-5}$ Torr	hexane+HF	1,327	19.1	3.19×10^{-15}	4000
	hexane+HF	19.1	13.4	3.34×10^{-15}	4000
	hexane+HF	1,412	13.4	3.14×10^{-15}	8000
0.2 Torr O_2	hexane+HF	1,327	????	no result ⁽¹⁾	4000
	hexane+HF	1,327	34.4	8.18×10^{-16}	8000
3.4 Torr O_2	hexane+HF	1,412	27.4	4.78×10^{-15}	4000
	hexane+HF	14.1	8.9	4.35×10^{-15}	4000
	hexane+HF	1,412	8.9	4.58×10^{-15}	8000

⁽¹⁾Wear rate could not be estimated due to poor wear scar definition in Figure 3.

Table 2. Wide temperature range wear rates of polished and chemically cleaned SiC-B sliding against itself in vacuum and 0.2 and 3.4 Torr P_{O_2} .

Atmosphere	Specimen Cleaning Method	Stress (MPa)		Pin Wear Rate ($m^3/N \cdot m$)	No. of cycles
		Start	End		
$\sim 1 \times 10^{-5}$ Torr	hexane+HF	1,412	25.6	2.40×10^{-15}	4000
	hexane+HF	31.2	20.0	6.61×10^{-16}	4000
	hexane+HF	1,412	20.0	1.53×10^{-15}	8000
0.2 Torr O_2	hexane+HF	1,412	????	no result ⁽¹⁾	4000
	hexane+HF	1,412	28.9	1.85×10^{-15}	8000
3.4 Torr O_2	hexane+HF	1,412	14.1	8.49×10^{-15}	4000
	hexane+HF	14.1	8.9	1.40×10^{-14}	4000
	hexane+HF	1,412	8.9	1.13×10^{-14}	8000

⁽¹⁾Wear rate could not be estimated due to poor wear scar definition.

Table 3. AES/XPS-measured atomic concentration of the hexane+HF-washed and 0.2 Torr O₂-tested Hexoloy SiC tribopin.

AES Survey Results (Tribopin P/N 980303-1/-4)

Location	Depth	Atomic Concentration				File #
		C	O	Si		
Wear Scar, Smooth Area	Surface	100				3
"	-5Å	82	4	14		5
Wear Scar, Rough Area	Surface	100				4
"	-5Å	94	6			6
"	-10 Å	98	2			7
Wear Scar, Large Area	-10Å	100				9
Wear Debris	Surface	62	19	19		1
Tip, Off-Scar	Surface	70	10	20		2
"	-10Å	54	14	33		8

XPS Survey Results (Tribopin P/N 980303-1/-4)

Location	Depth	Atomic Concentration				File #
		C	O	Na	Si	
Whole Tip	-10Å	63	14	1	23	10

XPS Multiplex Results (Tribopin P/N 980303-1/-4)

Location	Depth	High Resolution Spectral Data		
		C	O	Si
Whole Tip (includes Scar, Debris, and Unworn areas)	-10 Å	68 at%	14 at%	19 at%
		283.5 eV: 29.4%	531.9 eV: 100.0%	100.3 eV: 71.3%
		284.4 eV: 63.6%		102.1 eV: 28.7%
		287.0 eV: 7.0%		

Table 4. AES/XPS-measured atomic concentration of the hexane+HF-washed and 3.4 Torr O₂-tested Hexoloy SiC tribopin.

AES Survey Results (Tribopin P/N 990104-1/-4)

Location	Depth	Atomic Concentration					File #
		C	O	Si	N	S	
Wear Scar, Low Relief #1	Surface	57	8	35			2
Wear Scar, Low Relief #2	Surface	64	6	29			3
Wear Scar, Low Relief	-5Å	54	10	35			5
Wear Scar, High Relief	-5Å	42	30	28			6
Wear Debris	Surface	45	28	26			1
"	-5Å	31	43	26			7
Wear Debris, Fiber Rich	-5Å	56	16	26	2	<1	8
Tip, Off-Scar	-5Å	49	13	37		<1	9

XPS Survey Results (Tribopin P/N 990104-1/-4)

Location	Depth	Atomic Concentration					File #
		C	N	O	Na	Si	
Whole Tip	Surface	46	1	27	<1	25	4
"	-5Å	44		27		29	11

XPS Multiplex Results (Tribopin P/N 990104-1/-4)

Location	Depth	High Resolution Spectral Data		
		C	O	Si
Whole Tip (includes Scar, Debris, and Unworn areas)	-5Å	43 at%	28 at%	28 at%
		283.7 eV: 76.0%	532.2 eV: 24.8%	100.1 eV: 54.4%
		287.0 eV: 24.0%	535.2 eV: 75.2%	102.5 eV: 11.5%
				105.8 eV: 34.1%

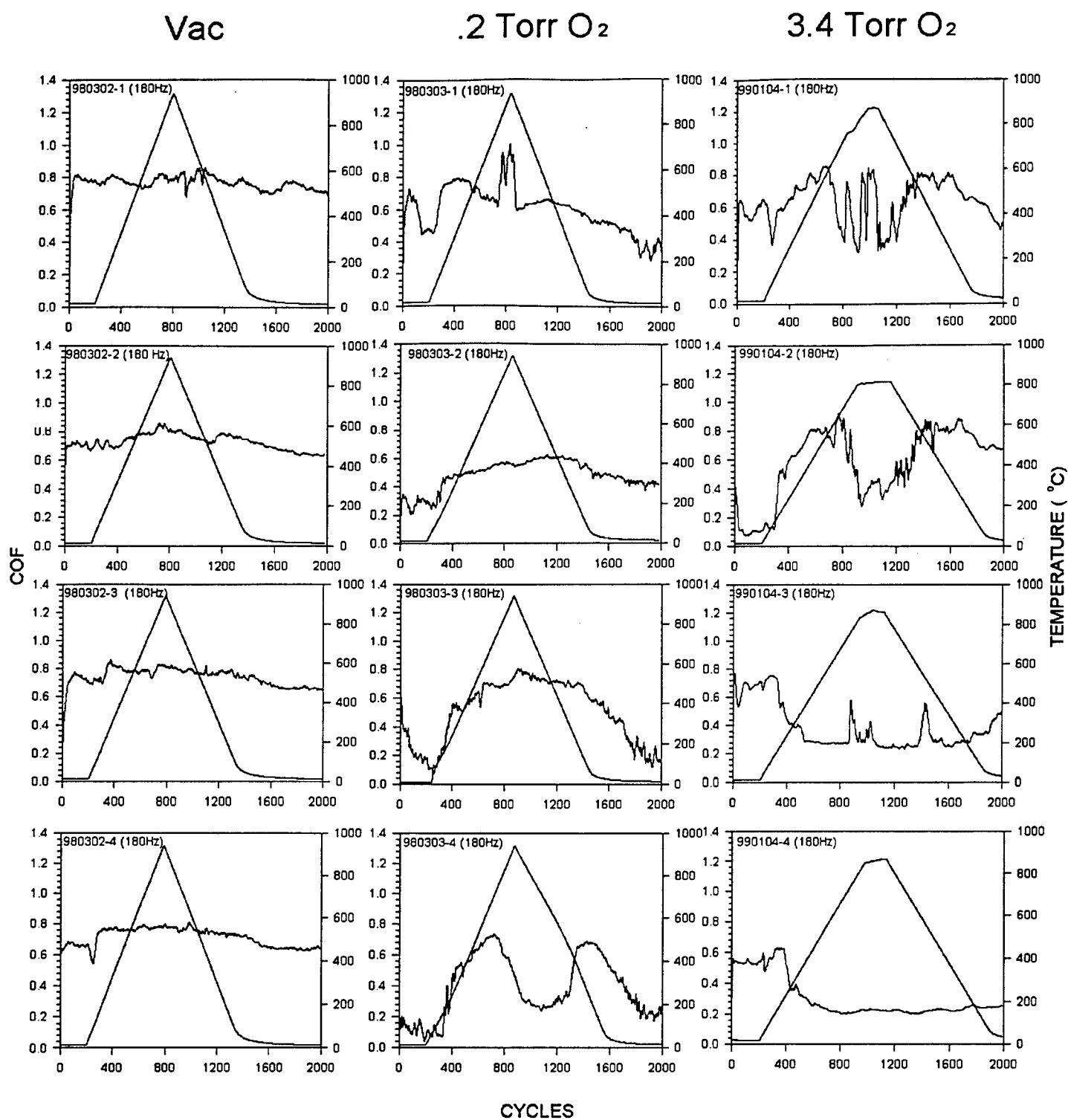


Figure 1. COF of hexane+HF-washed Hexoloy SiC in vacuum, 0.2 Torr and 3.4 Torr P_{O2}.

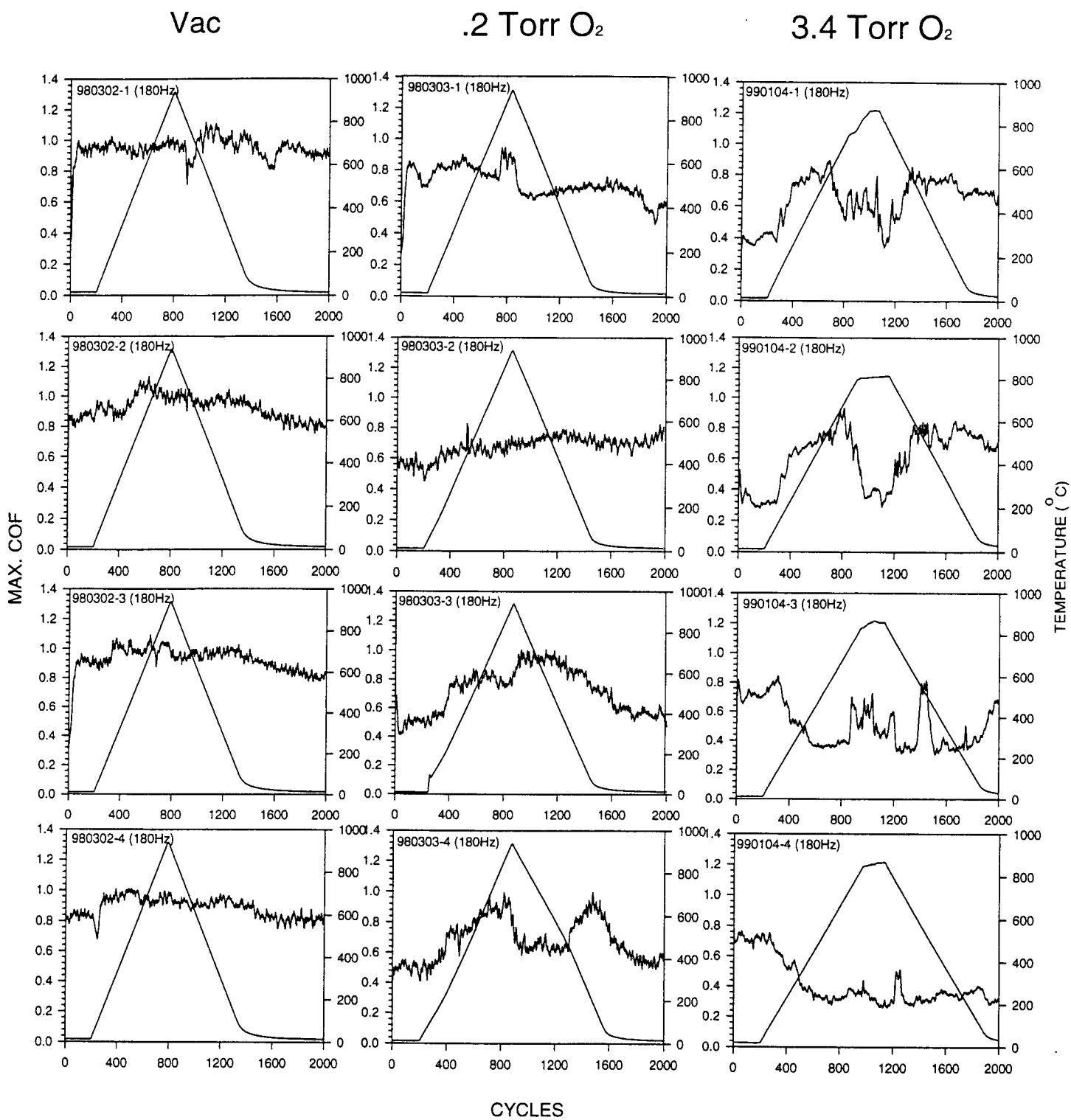


Figure 2. MAX.COF of hexane+HF-washed Hexoloy SiC in vacuum, 0.2 Torr and 3.4 Torr P_{O₂}.

Hexoloy SiC pin (hexane+HF-cleaned)

0.2 Torr O₂

3.4 Torr O₂

2 passes
in
Track 1
(as-tested)

4 passes
in
Tracks 1+2
(as-tested)

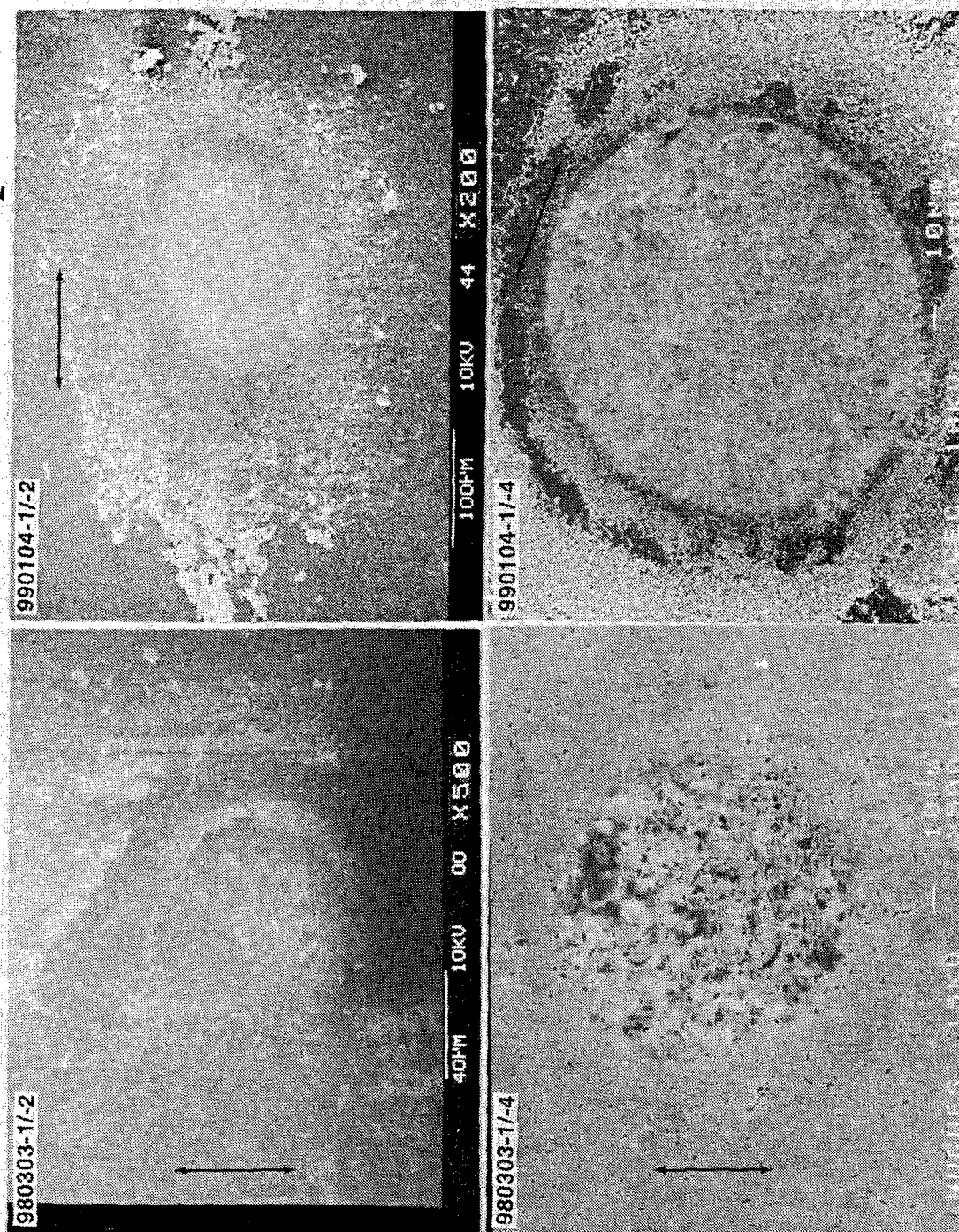
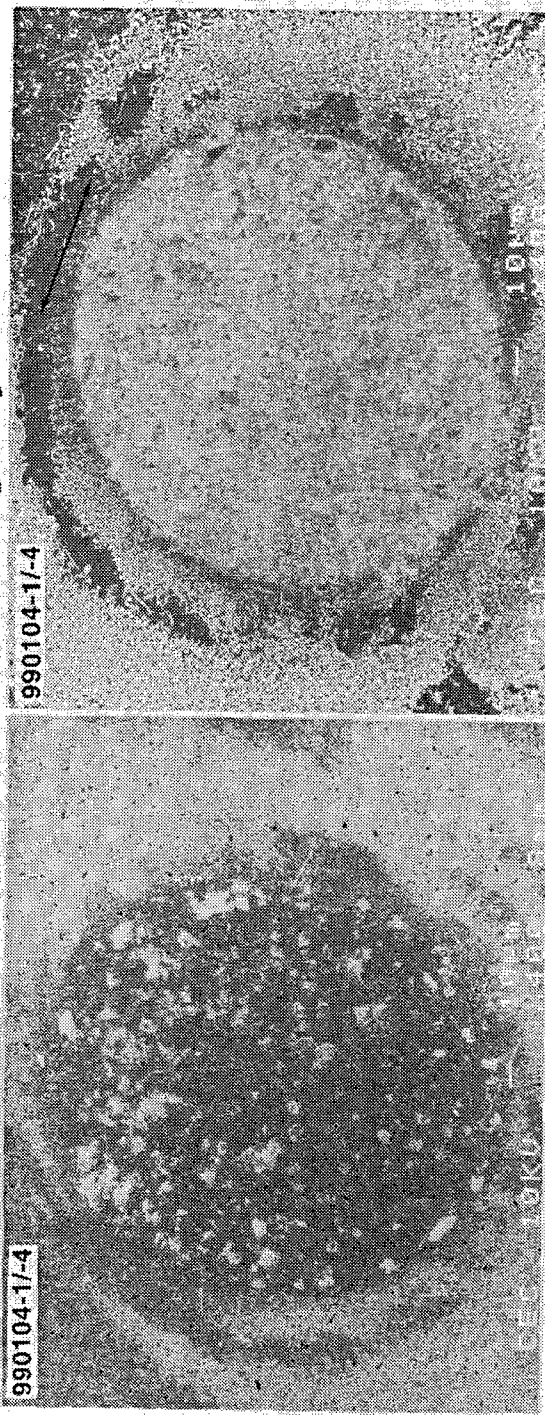


Figure 3. Normal incidence SEM photomicrographs of hexane+HF-washed Hexoloy SiC pin wear scars, as-tested in 0.2 and 3.4 Torr P_{O₂}; double-headed arrows indicate direction of sliding.

**Hexoloy SiC pin (3.4 Torr O₂; hexane+HF-cleaned)
on C/L**



**4 passes
in
Tracks 1+2
(as-tested)**

Figure 4. SEM photomicrographs of hexane+HF-washed Hexoloy SiC pin wear scar and wear debris, as-tested in 3.4 Torr PO₂; photo taken on-centerline (left) and slightly off-centerline (right) to show ovality of the scar as a function of photo angle.

Hexoloy SiC pin (hexane+HF-cleaned)

0.2 Torr O₂ 3.4 Torr O₂

4 passes
in
Tracks 1+2
(as-tested)

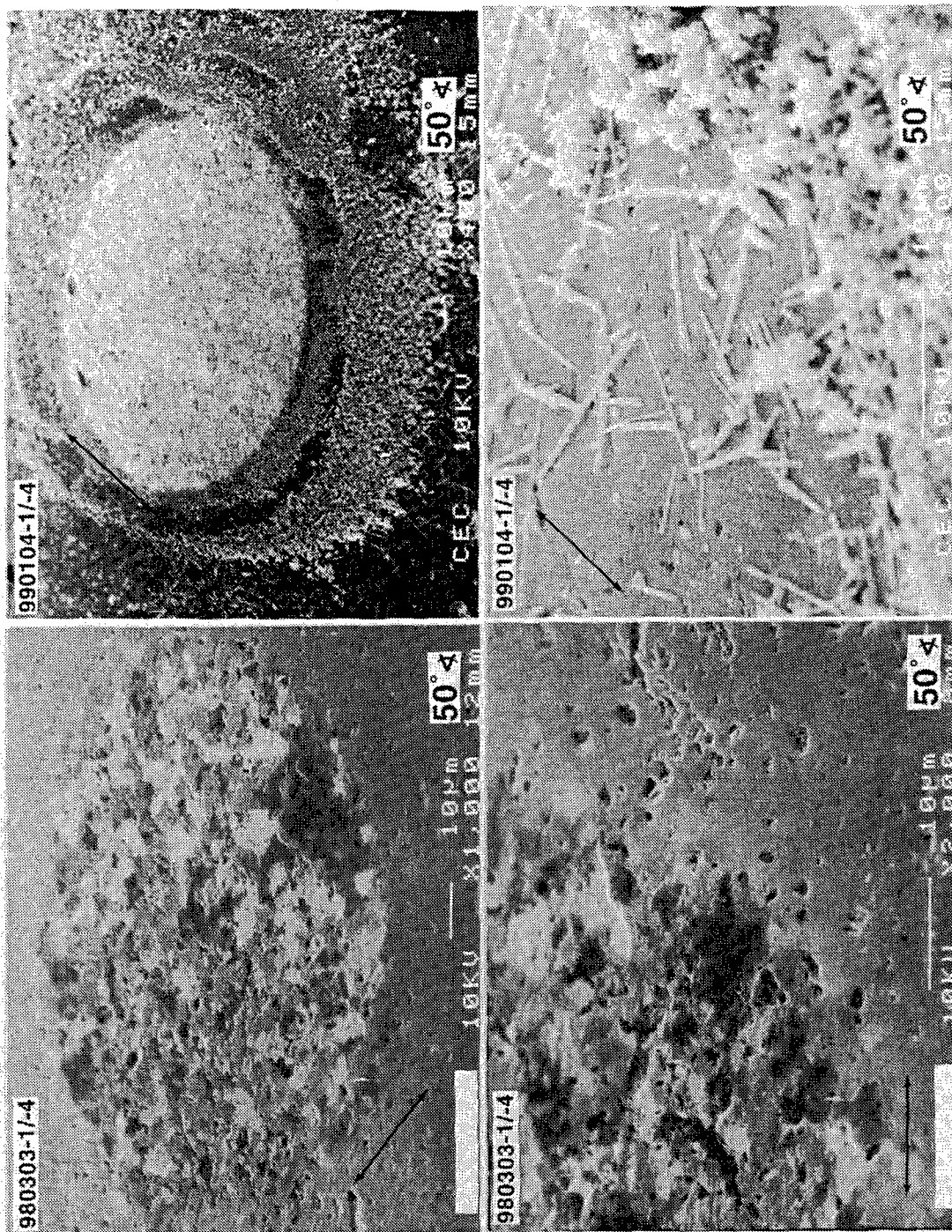


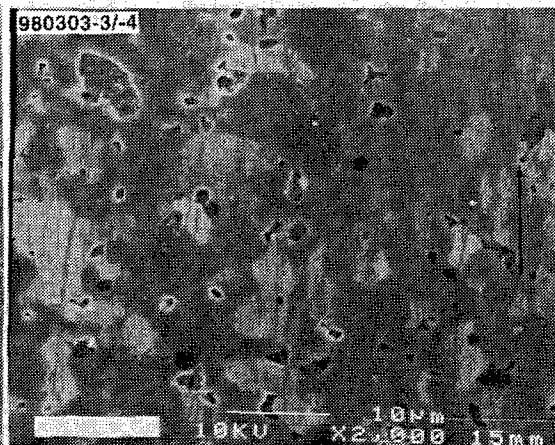
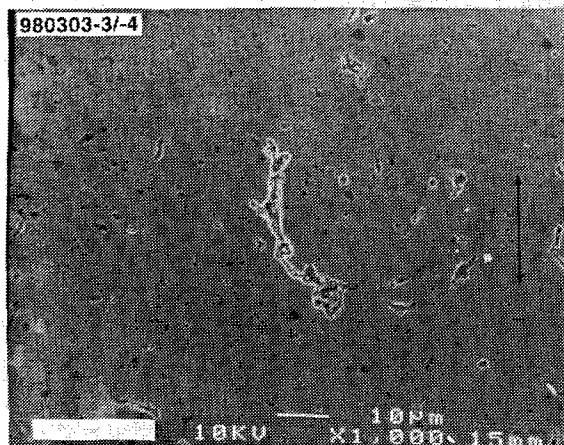
Figure 5. Shallow angle SEM photomicrographs of the hexane+HF-washed Hexoloy SiC pin wear scar edge, as-tested in 0.2 Torr and 3.4 Torr P_{O₂}, showing the scar texture and wear debris morphologies, at various magnifications. Double-headed arrows indicate direction of sliding.



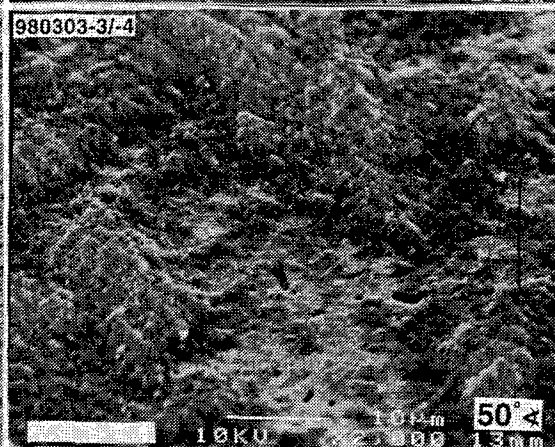
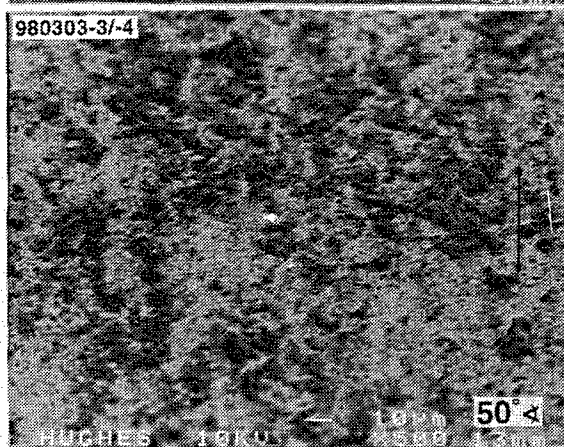
Figure 6. Normal incidence SEM photomicrographs of hexane+HF-washed Hexoloy SiC flat wear scars, as-tested in 0.2 Torr PO₂, showing early scar texture and wear debris morphologies; double-headed arrows indicate direction of sliding.

Hexoloy SiC flat (0.2 Torr O₂; hexane+HF-cleaned)

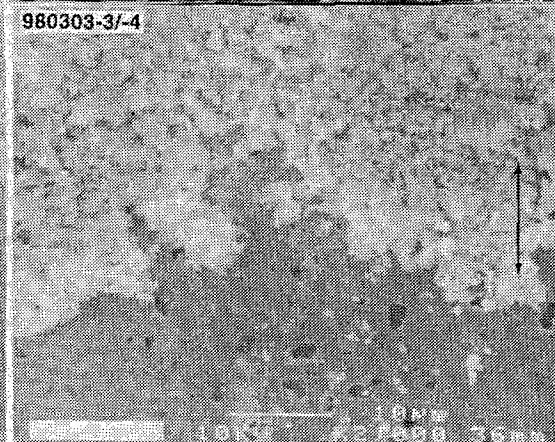
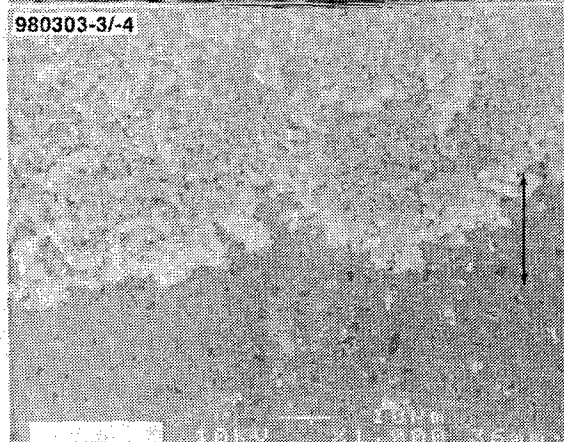
smooth
scar
area



rough
scar
area



track
end
debris

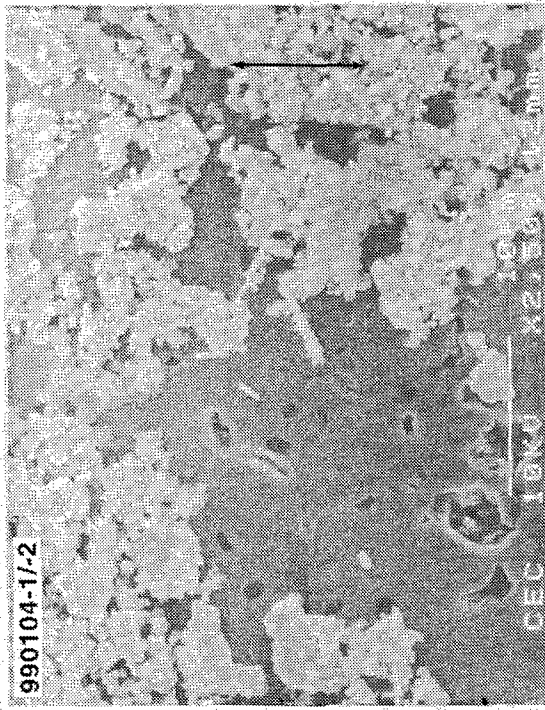
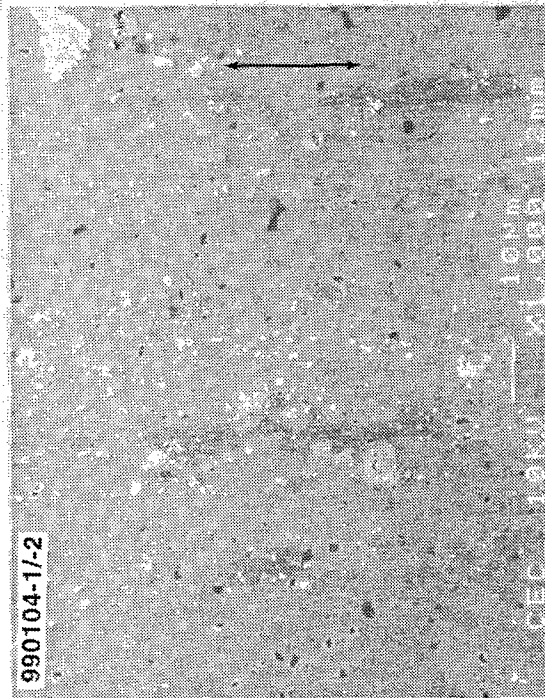


2 passes in Track 2 (as-tested)

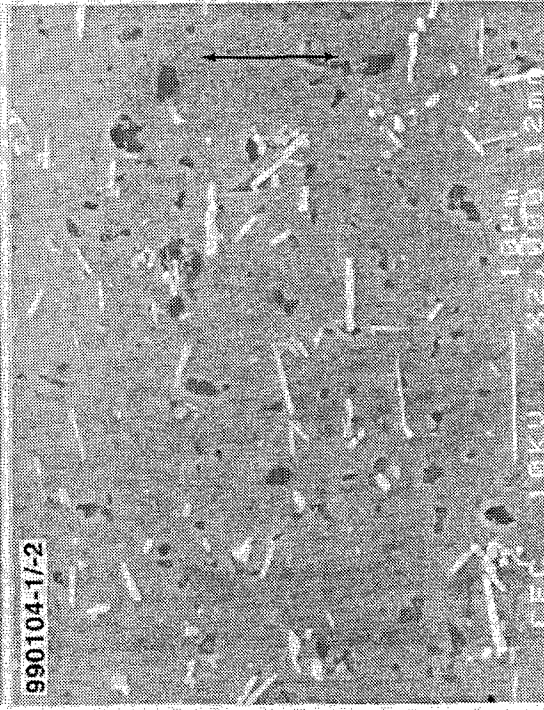
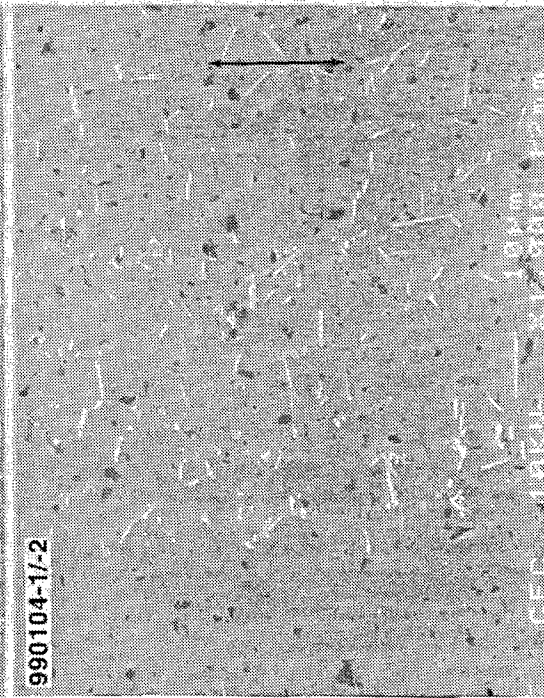
Figure 7. Normal incidence SEM photomicrographs of hexane+HF-washed Hexoloy SiC flat wear scars, as-tested in 0.2 Torr P_O₂, showing mature scar textures and wear debris morphologies; double-headed arrows indicate direction of sliding.

Hexoloy SiC flat (3.4 Torr O₂; hexane+HF-cleaned)

scar
(middle)



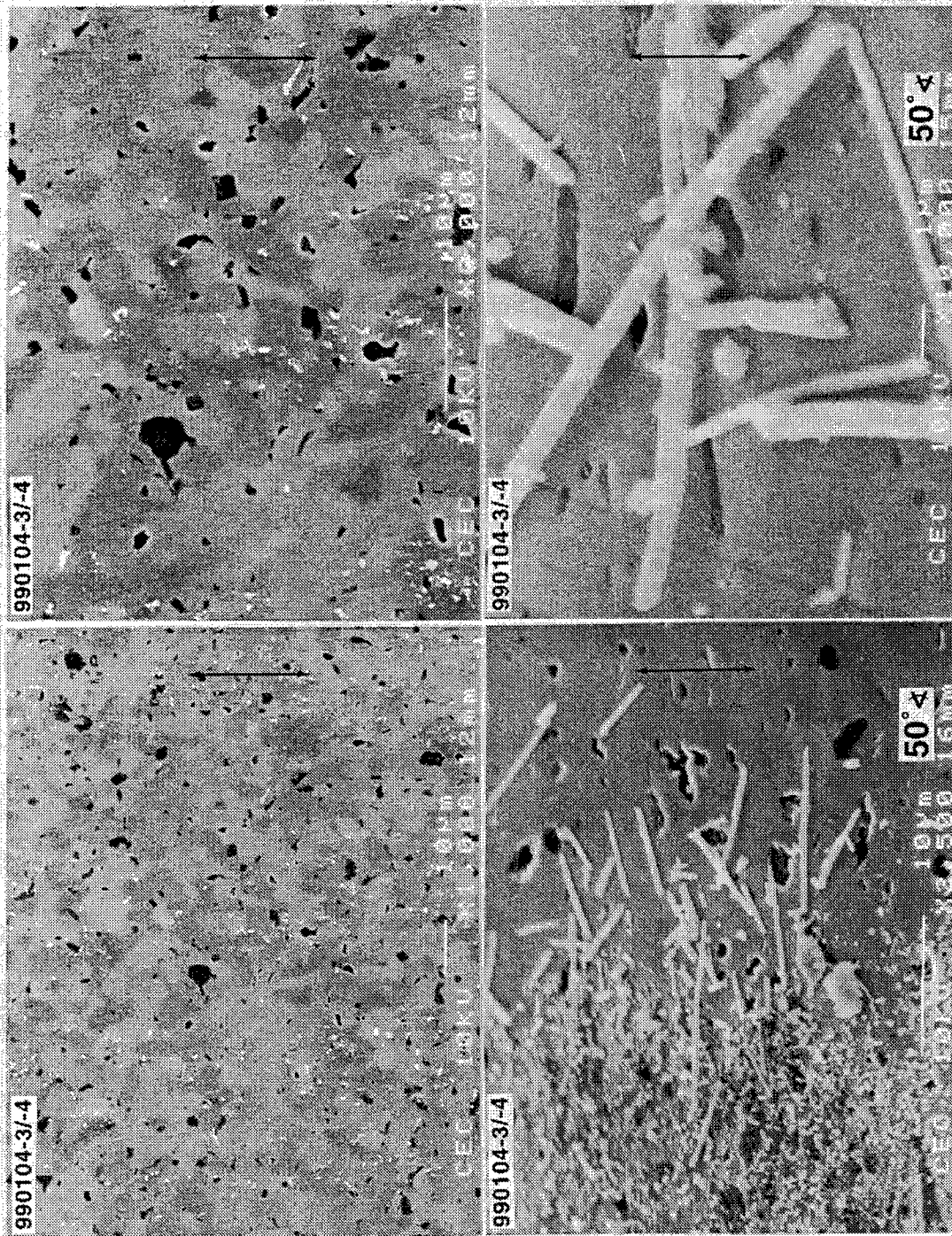
scar
(side)



2 passes in Track 1 (as-tested)

Figure 8. Normal incidence SEM photomicrographs of hexane+HF-washed Hexoloy SiC flat wear scars, as-tested in 3.4 Torr PO₂, showing early scar textures and wear debris morphologies; double-headed arrows indicate direction of sliding.

Hexoloy SiC flat (3.4 Torr O₂; hexane+HF-cleaned)



2 passes in Track 2 (as-tested)

Figure 9. Normal incidence SEM photomicrographs of hexane+HF-washed Hexoloy SiC flat wear scars, as-tested in 3.4 Torr P_{O₂}, showing mature scar textures and wear debris morphologies; double-headed arrows indicate direction of sliding.

Hexoloy SiC (3.4 Torr O₂)



SiC-B (3.4 Torr O₂)

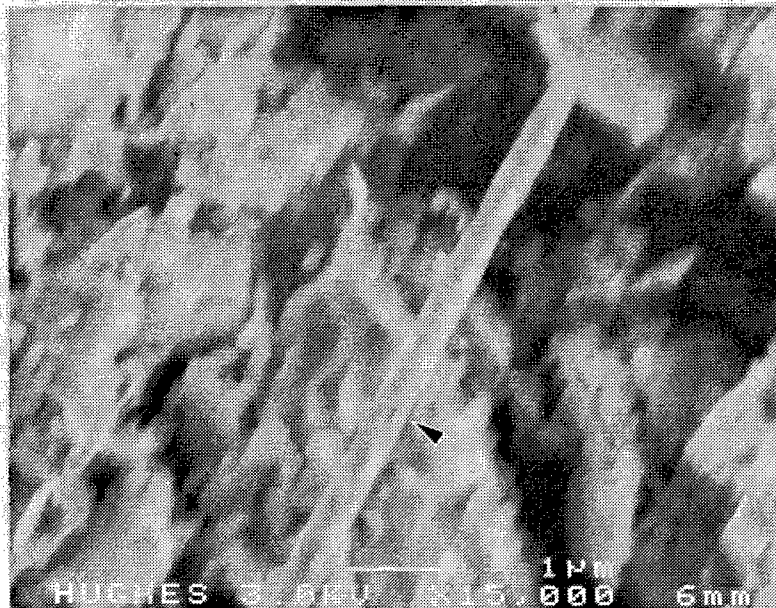


Figure 10. Similarities in the "rolling pin" wear debris appearance of Hexoloy SiC and CERCOM SiC-B.

Hexoloy SiC pin (hexane+HF-cleaned)

0.2 Torr O₂

3.4 Torr O₂

4 passes
in
Tracks 1+2
(as-tested)

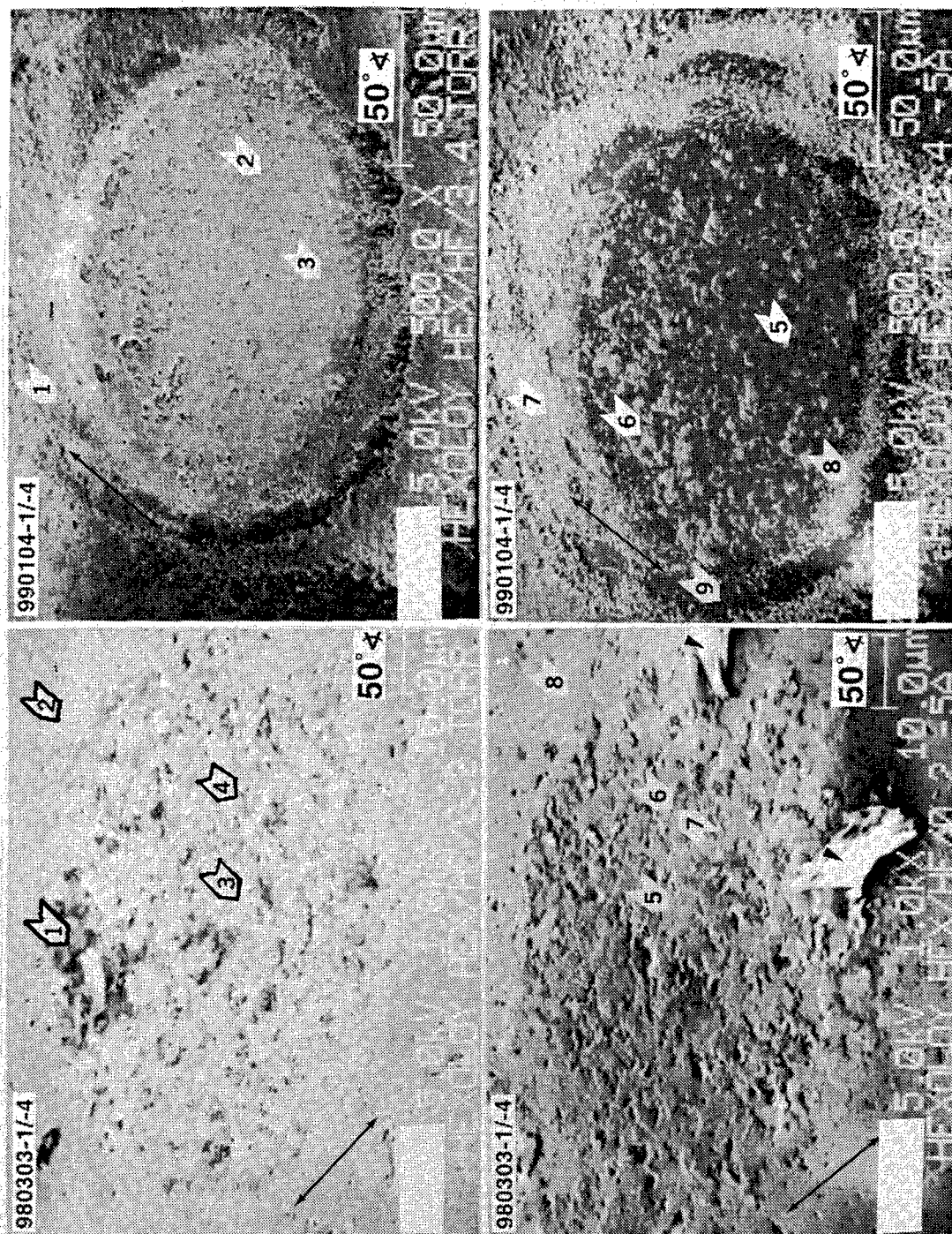


Figure 11. Shallow angle SAM photomicrographs of the hexane+HF-washed Hexoloy SiC pin wear scar, as-tested in 0.2 Torr and 3.4 Torr O₂ (arrows indicate analytical sites); various magnifications (also see Tables 3 and 4).

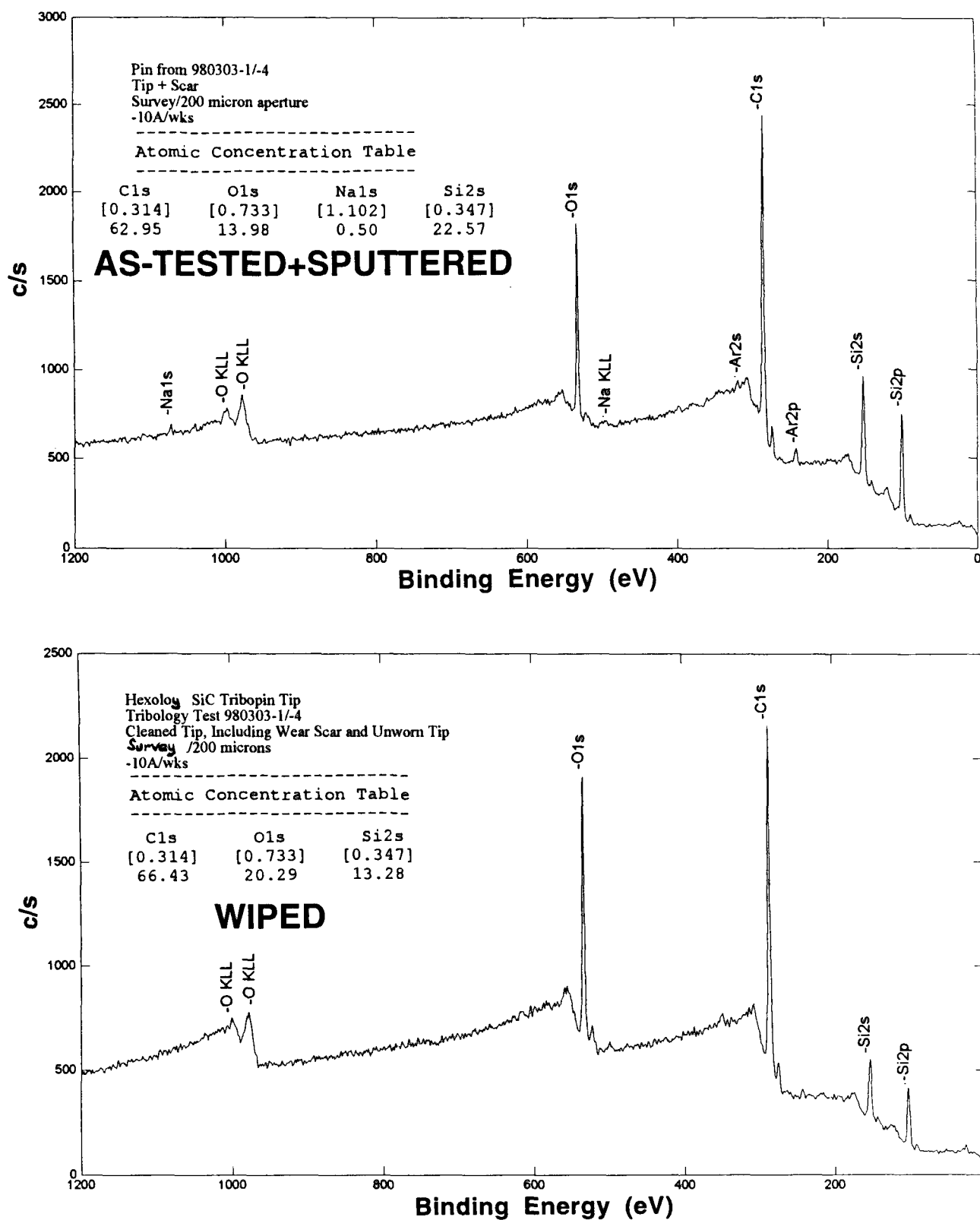


Figure 12. Wide-scan survey XPS spectra of the hexane+HF-washed and 0.2 Torr PO_2 -tested Hexoloy SiC pin tip wear scar, in the as-tested+Ar-sputtered (top) and wiped+Ar-sputtered (bottom) conditions; also see Table 3. Ar-sputtering removed 1 nm in each case.

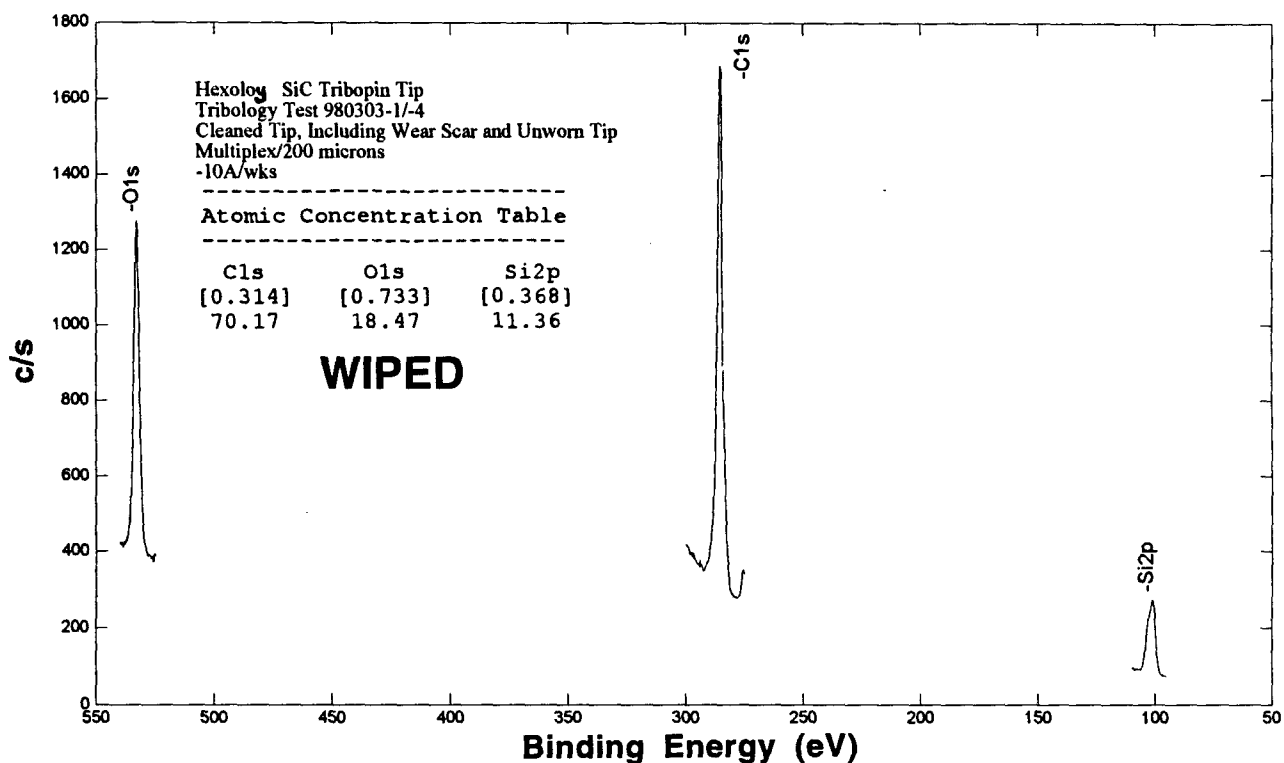
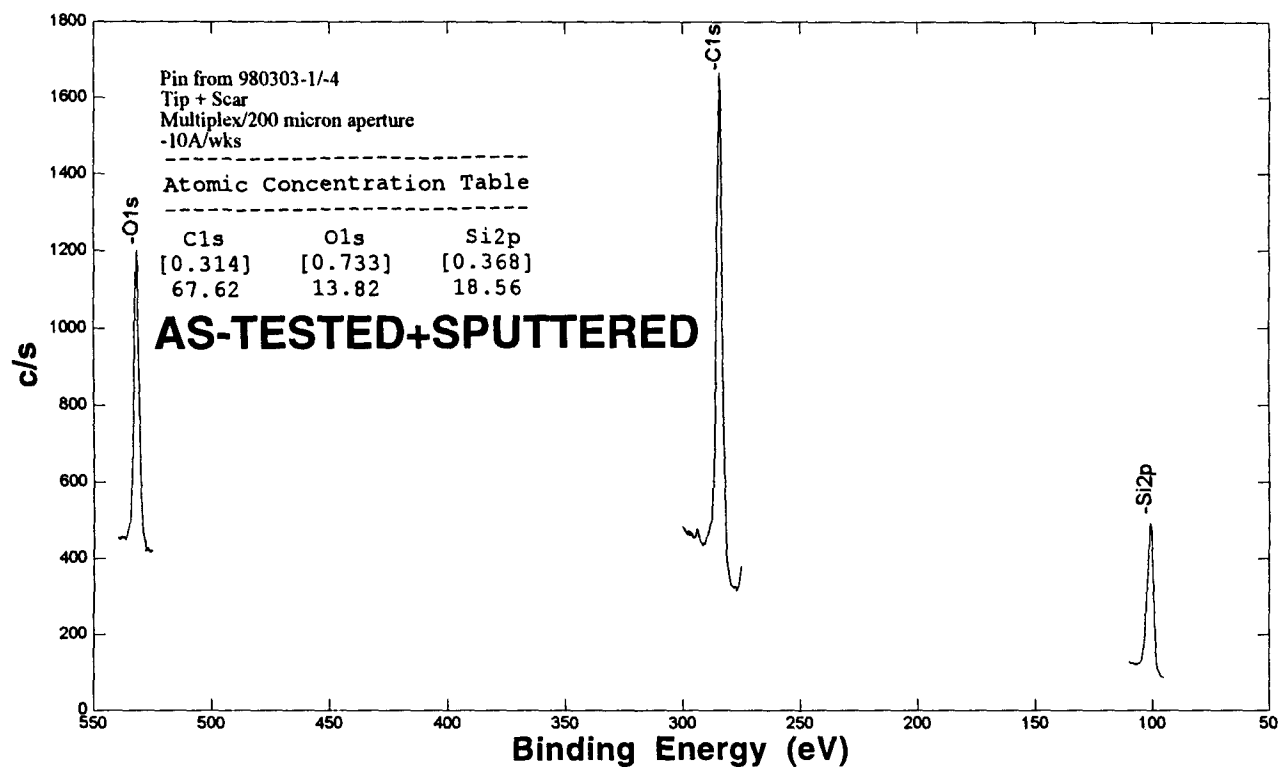


Figure 13. Multiplexed XPS spectra of the hexane+HF-washed and 0.2 Torr PO₂-tested Hexoloy SiC pin tip wear scar, in the as-tested+Ar-sputtered (top) and wiped+Ar-sputtered (bottom) conditions; also see Table 3. Ar-sputtering removed 1 nm in each case.

HEXOLOY-SiC (0.2 Torr O₂; AS-TESTED+SPUTTERED)

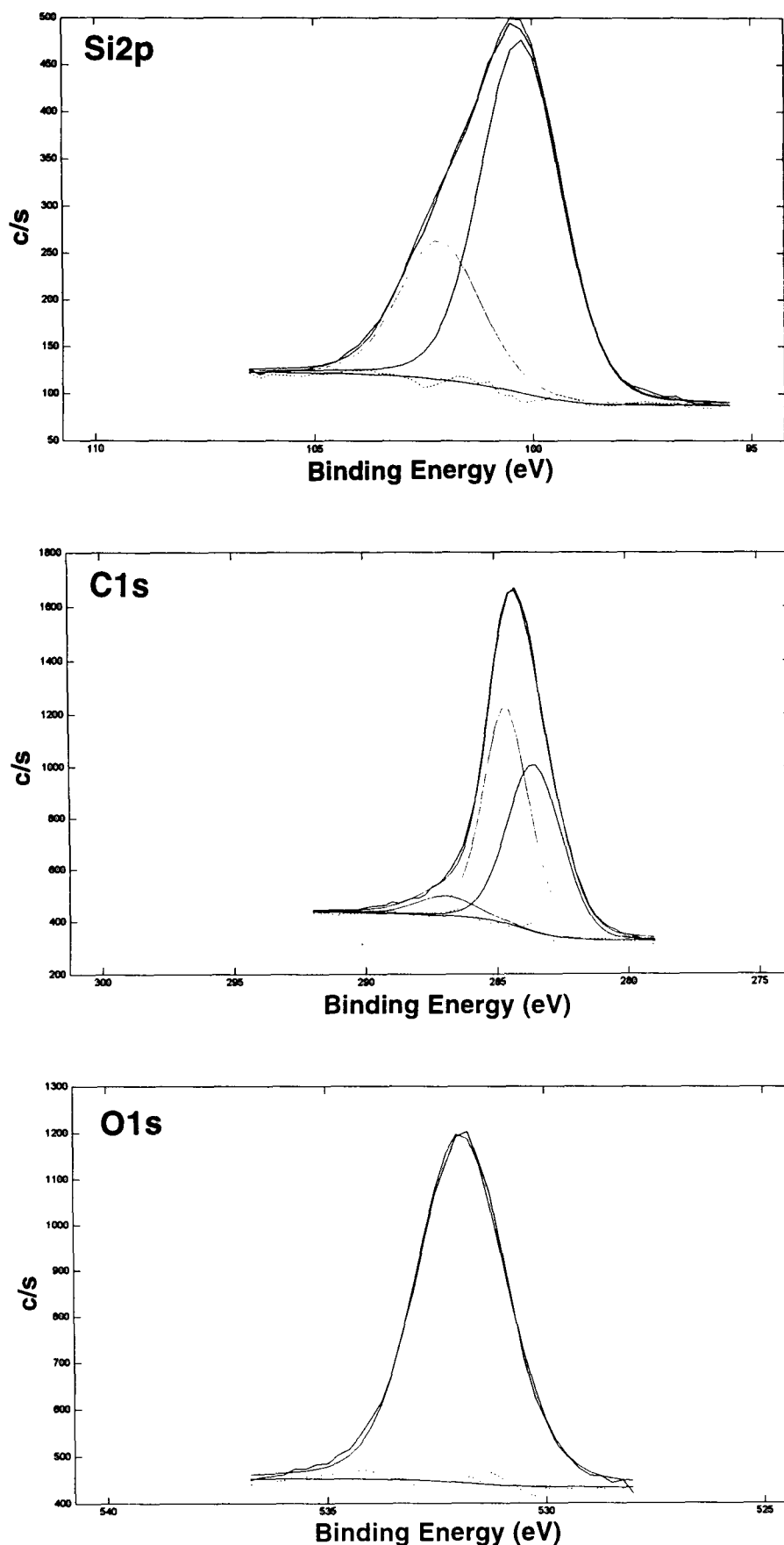


Figure 14. Deconvoluted Si, C and O spectral peaks of hexane+HF-washed and 0.2 Torr PO₂-tested Hexoloy SiC pin tip wear scar, in the as-tested+Ar-sputtered condition (also see Table 3). Ar-sputtering removed 1 nm. Peak assignments: Si2p peaks: 100.0 eV = carbidic, 102.2 eV = Si-O, silicates; C1s peaks: 282.7 eV = carbidic, 284.6 eV = graphitic, 286.7 eV = C-O, C=O; O1s peak: 532.0 eV = O-Si, organic carbonyls.

HEXOLOY-SiC (0.2 Torr O₂; WIPED+SPUTTERED)

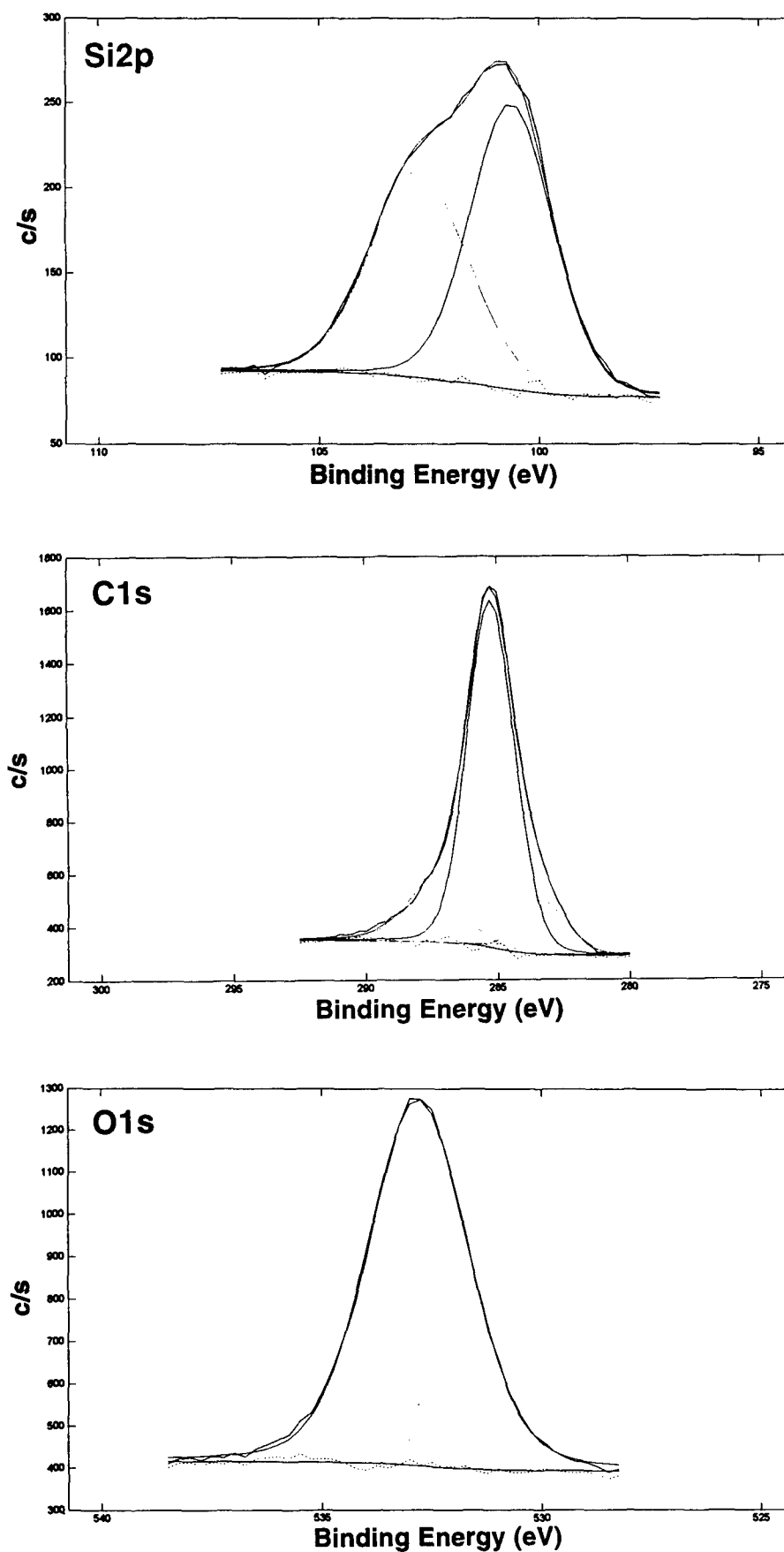


Figure 15. Deconvoluted Si, C and O spectral peaks of hexane+HF-washed and 0.2 Torr PO₂-tested Hexoloy SiC pin tip wear scar, in the wiped+Ar-sputtered condition (also see Table 3). Ar-sputtering removed 1 nm. Peak assignments: Si2p peaks: 100.0 eV = carbidic, 102.2 eV = Si-O, silicates; C1s peaks: 282.7 eV = carbidic, 284.6 eV = graphitic, 286.7 eV = C-O, C=O; O1s peak: 532.0 eV = O-Si, organic carbonyls.

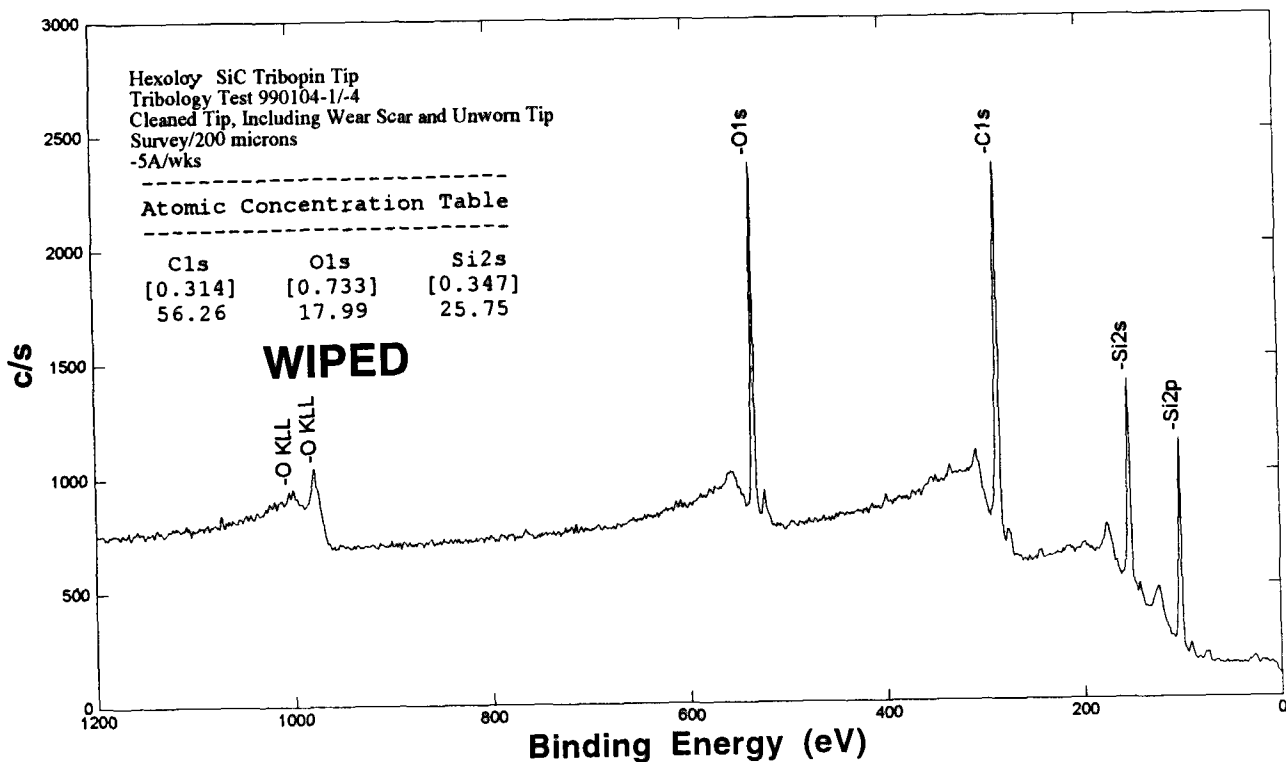
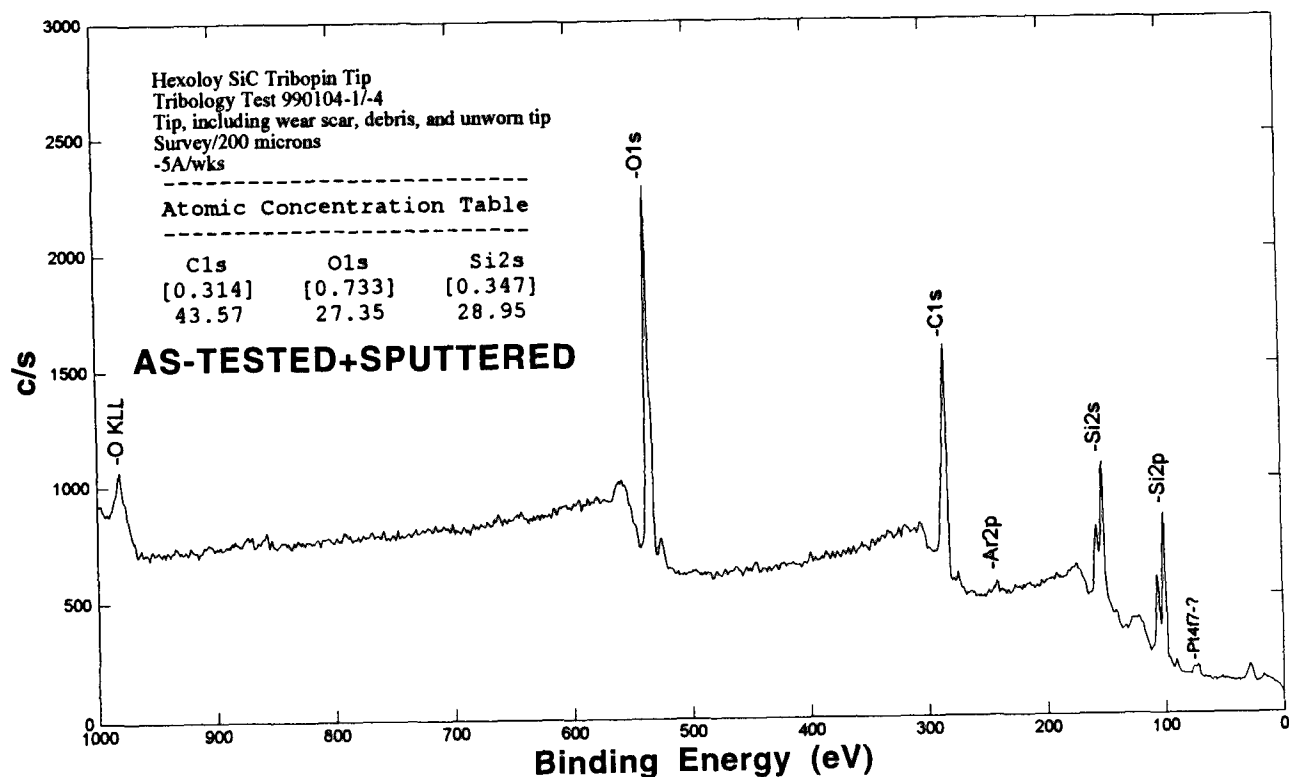


Figure 16. Wide-scan survey XPS spectra of the hexane+HF-washed and 3.4 Torr PO_2 -tested Hexoloy SiC pin tip wear scar, in the as-tested+Ar-sputtered (top) and wiped+Ar-sputtered (bottom) conditions; also see Table 4). Ar-sputtering removed 0.5 nm in each case.

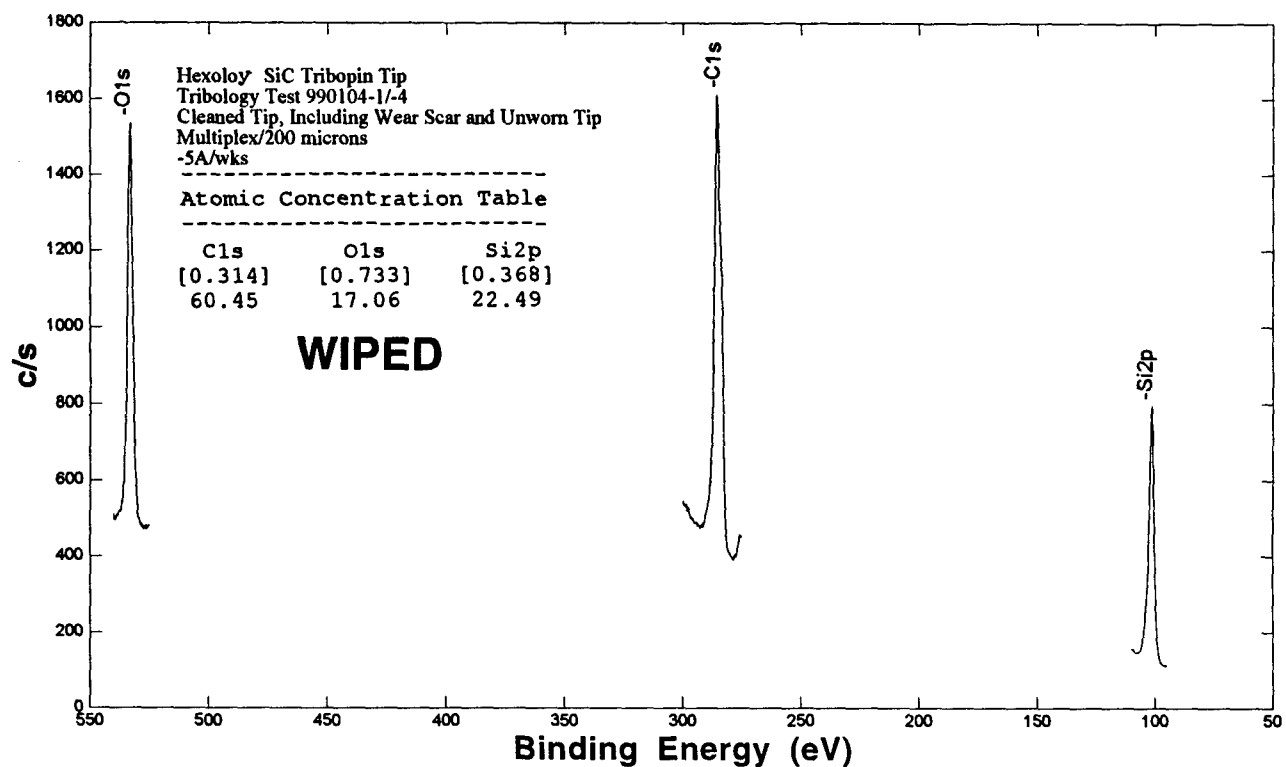
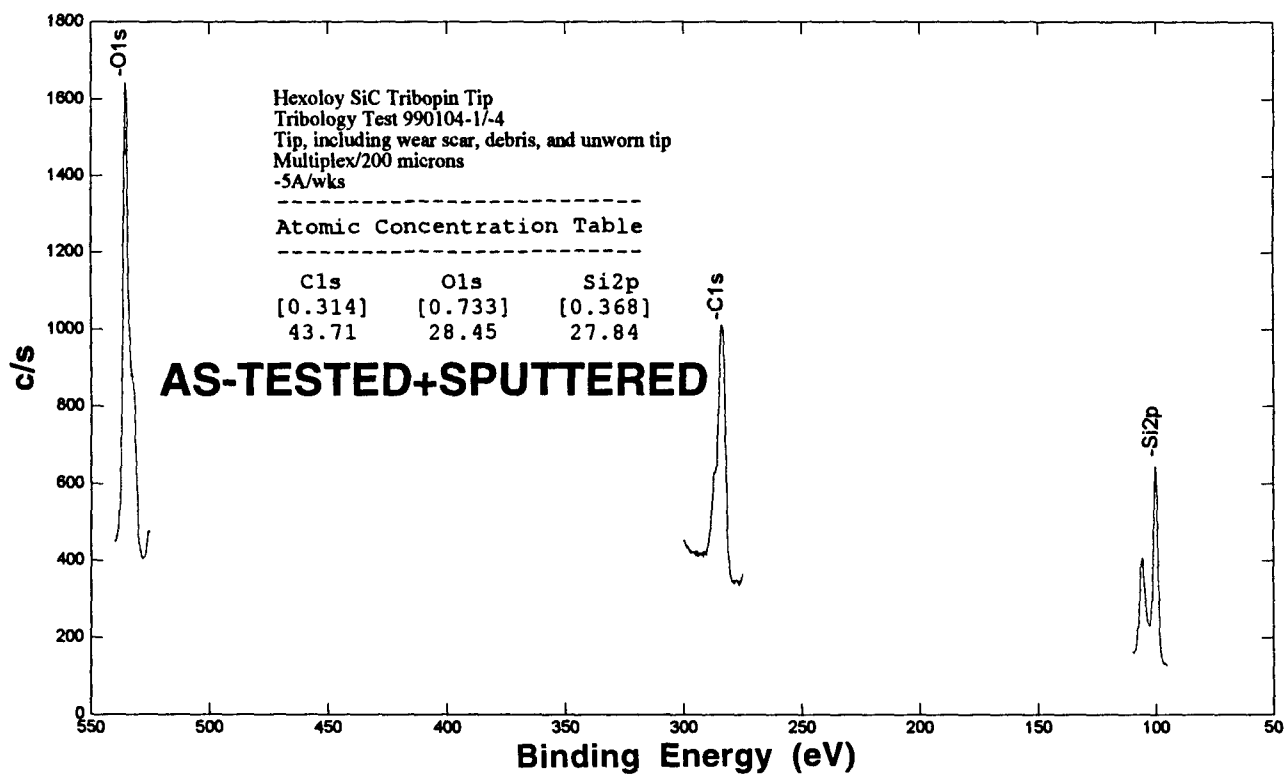


Figure 17. Multiplexed XPS spectra of the hexane+HF-washed and 3.4 Torr PO_2 -tested Hexoloy SiC pin tip wear scar, in the as-tested+Ar-sputtered (top) and wiped+Ar-sputtered (bottom) conditions; also see Table 4. Ar-sputtering removed 0.5 nm in each case.

HEXOLOY-SiC (3.4 Torr O₂; AS-TESTED+SPUTTERED)

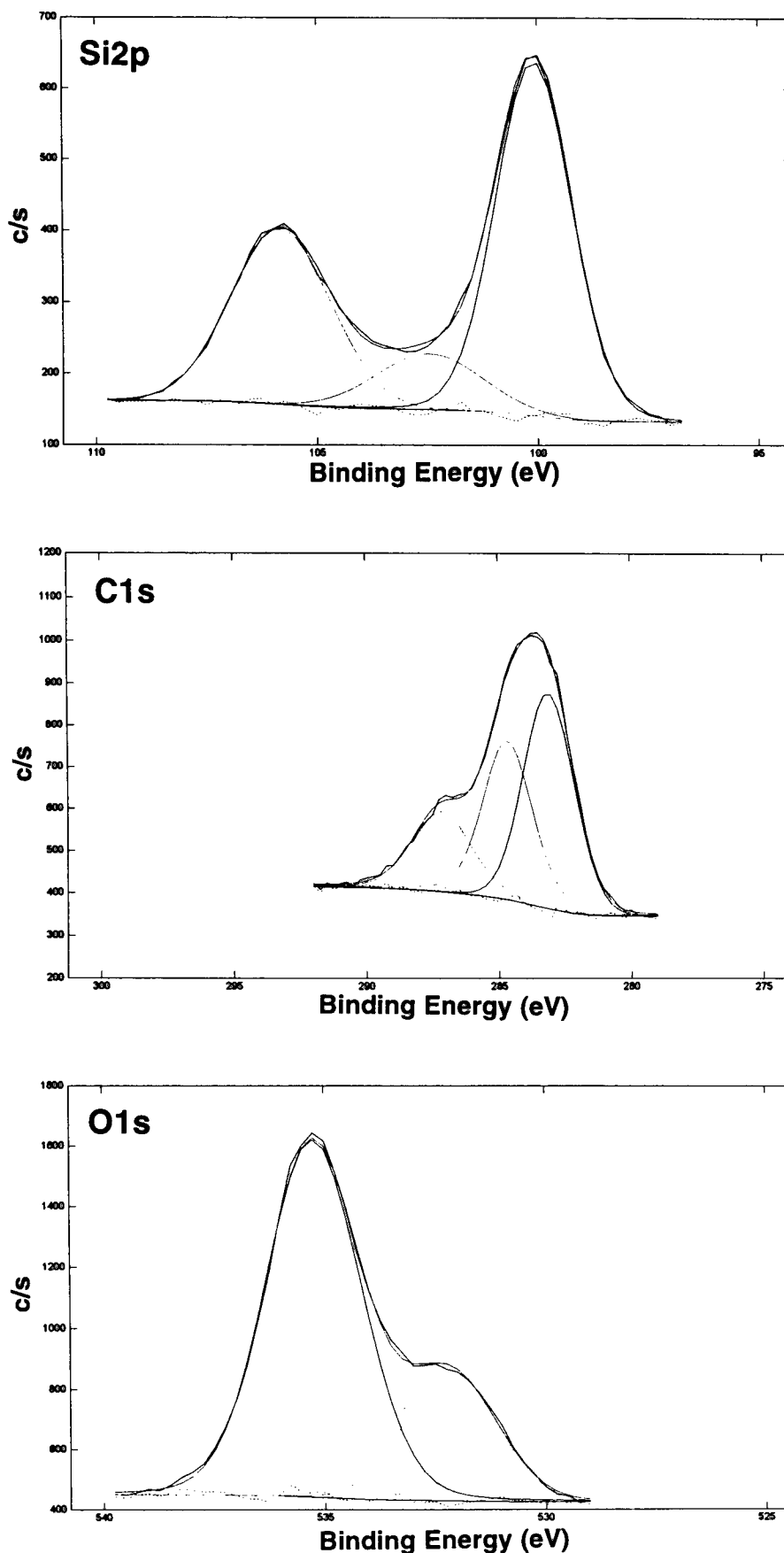


Figure 18. Deconvoluted Si, C and O spectral peaks of hexane+HF-washed and 3.4 Torr P_{O2}-tested Hexoloy SiC pin tip wear scar, in the wiped+Ar-sputtered condition (also see Table 4). Ar-sputtering removed 0.5 nm. Peak assignments: Si2p peaks: 100.0 eV = carbidic, 102.2 eV = Si-O, silicates, 105.8 eV = anomalously high value; C1s peaks: 282.7 eV = carbidic, 284.6 eV = graphitic, 286.7 eV = C-O, C=O; O1s peaks : 532.0 eV = O-Si, organic carbonyls, 535.2 eV = anomalously high value.

HEXOLOY-SiC (3.4 Torr O₂; AS-TESTED+SPUTTERED)

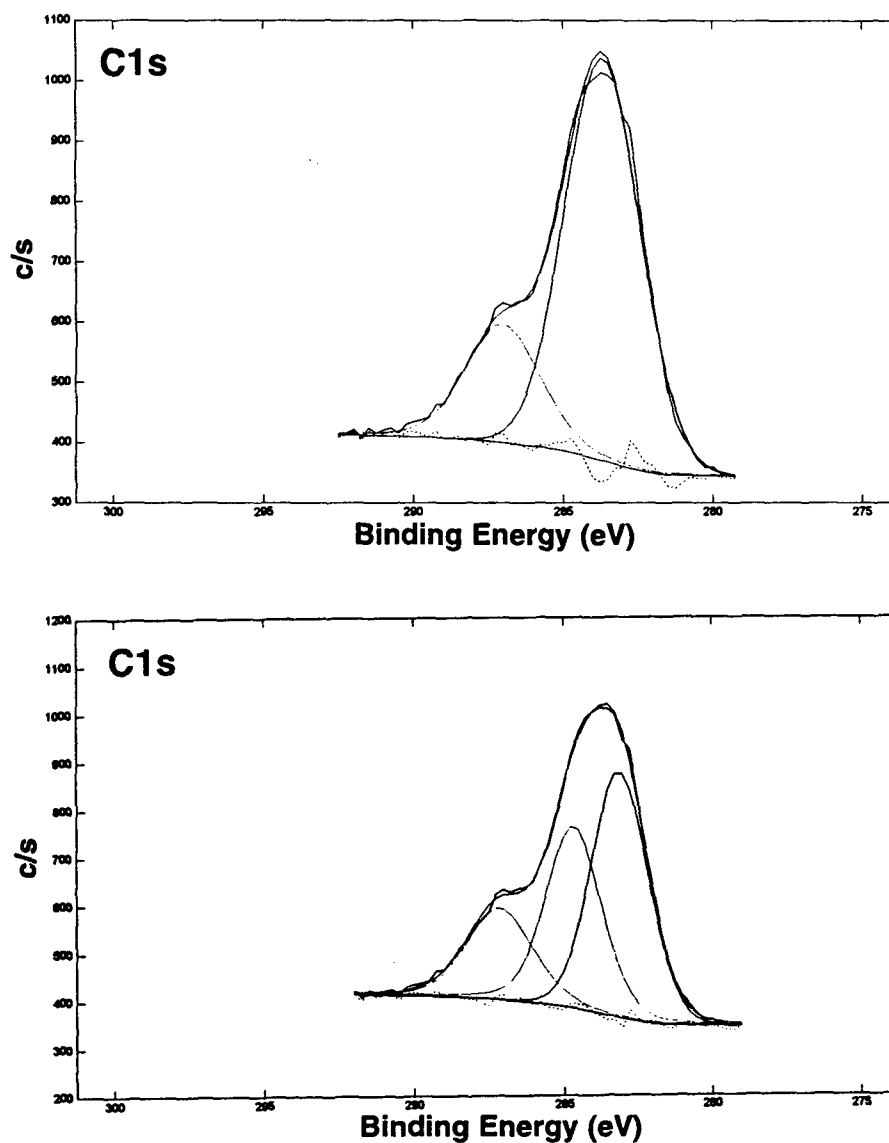


Figure 19. Improved deconvolution of the C1s spectral peak of hexane+HF-washed and 3.4 Torr PO₂-tested Hexoloy SiC pin tip wear scar, in the as-tested+Ar-sputtered condition. Ar-sputtering removed 0.5 nm. The dotted error function is significantly smoothed by incorporating the third peak.

HEXOLLOY-SiC (3.4 Torr O₂; WIPED+SPUTTERED)

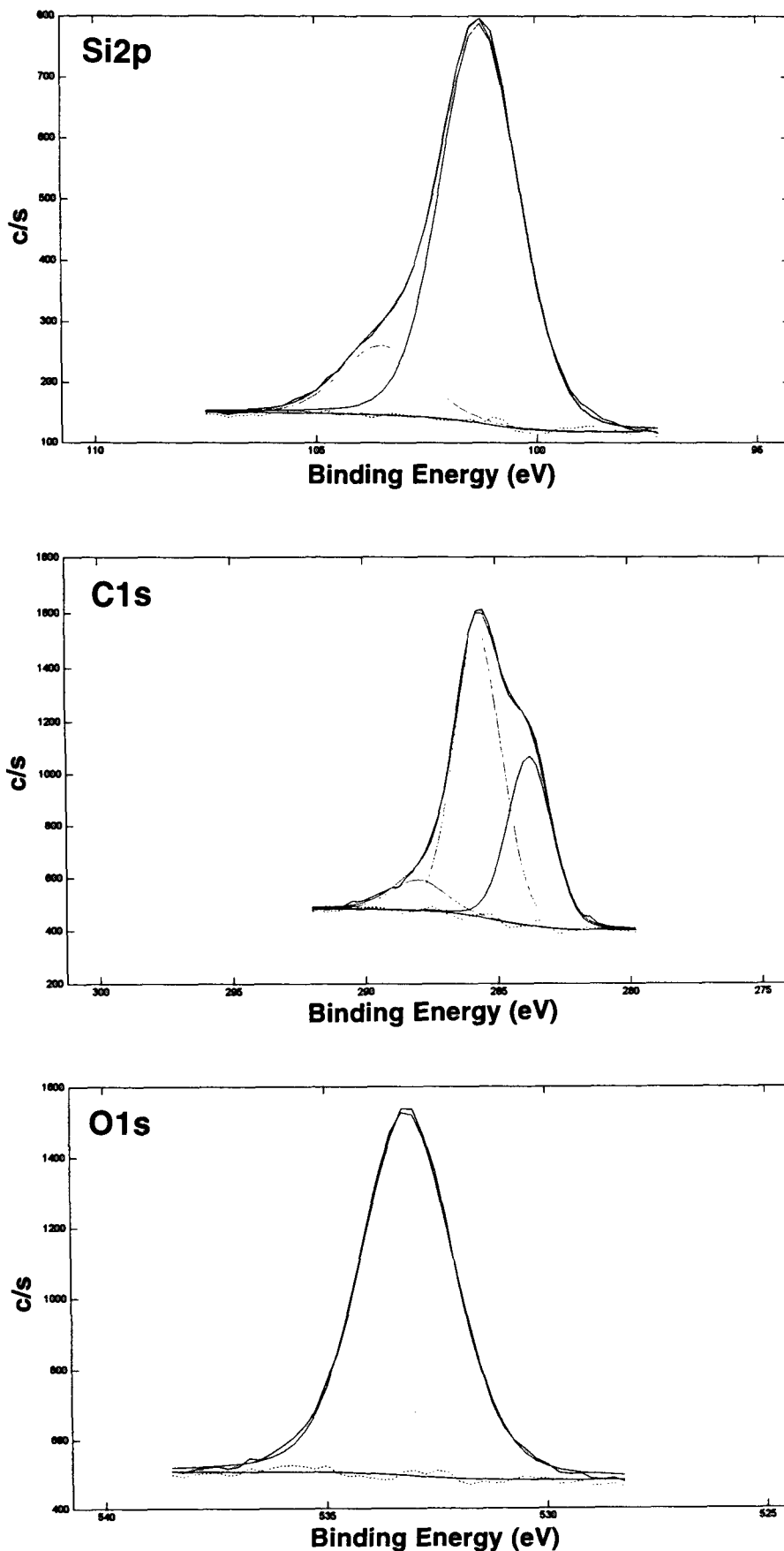


Figure 20. Deconvoluted Si, C and O spectral peaks of hexane+HF-washed and 3.4 Torr PO₂-tested Hexolloy SiC pin tip wear scar, in the wiped+Ar-sputtered condition (also see Table 4). Ar-sputtering removed 1 nm. Peak assignments: Si2p peaks: 100.0 eV = carbide, 102.2 eV = Si-O, silicates; C1s peaks: 282.7 eV = carbide, 284.6 eV = graphitic, 286.7 = C-O, C=O; O1s peaks : 532.0 eV = O-Si, organic carbonyls.

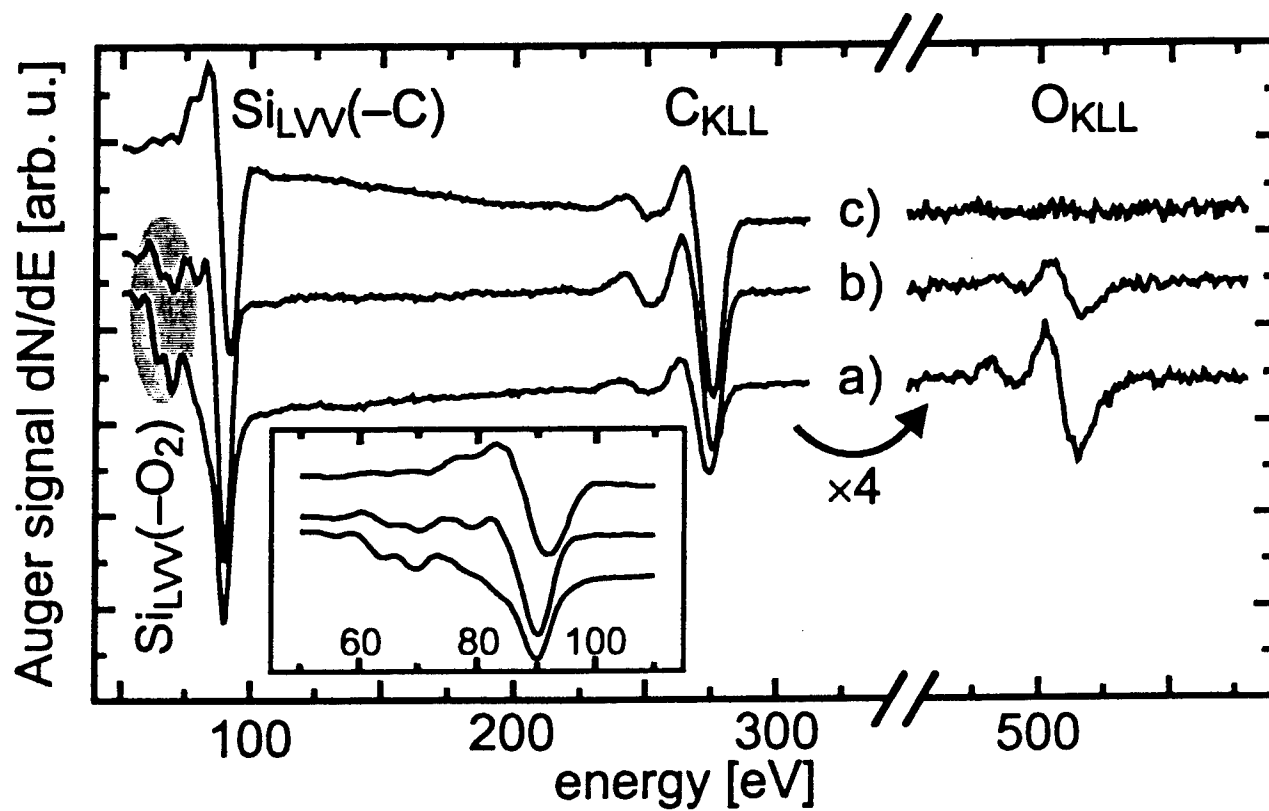


Figure 21. Auger spectra of the oxide $(\sqrt{3} \times \sqrt{3})R30^\circ$ structures on both crystal orientations [(a): SiC(0001); (b) SiC(000 $\bar{1}$)]. Both spectra display an oxygen peak as well as oxygen-related features in the Si_{LVV} peak (shown with enlarged energy scale in the inset). These features vanish when heating the sample at 1050°C [e.g., (c): (000 $\bar{1}$) surface]; from [2].

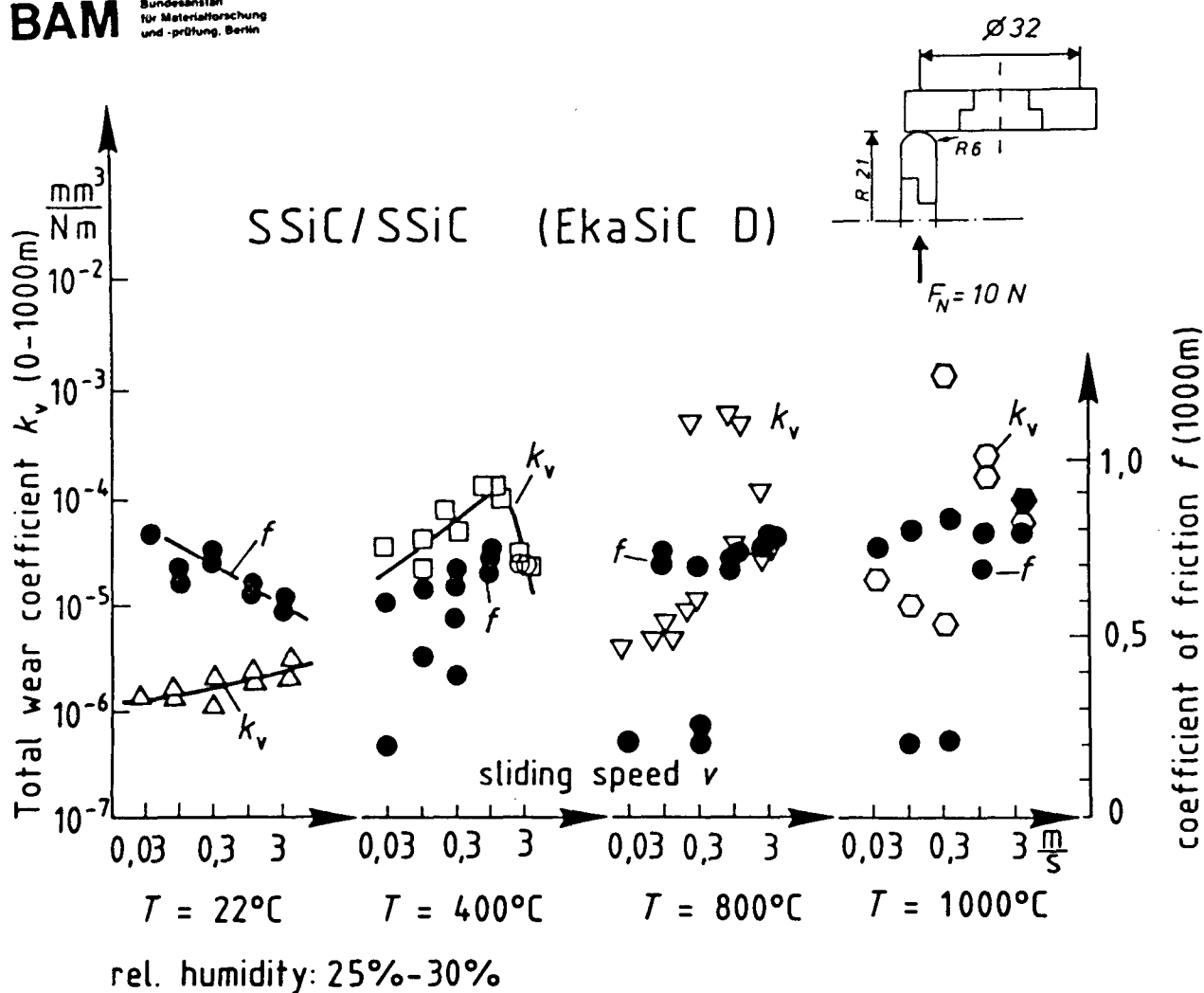


Figure 22. Friction (f) and wear rate (k_w) of a sintered SiC sliding against itself in air, at various speeds and temperatures (pin-on-disc test configuration); from [3].

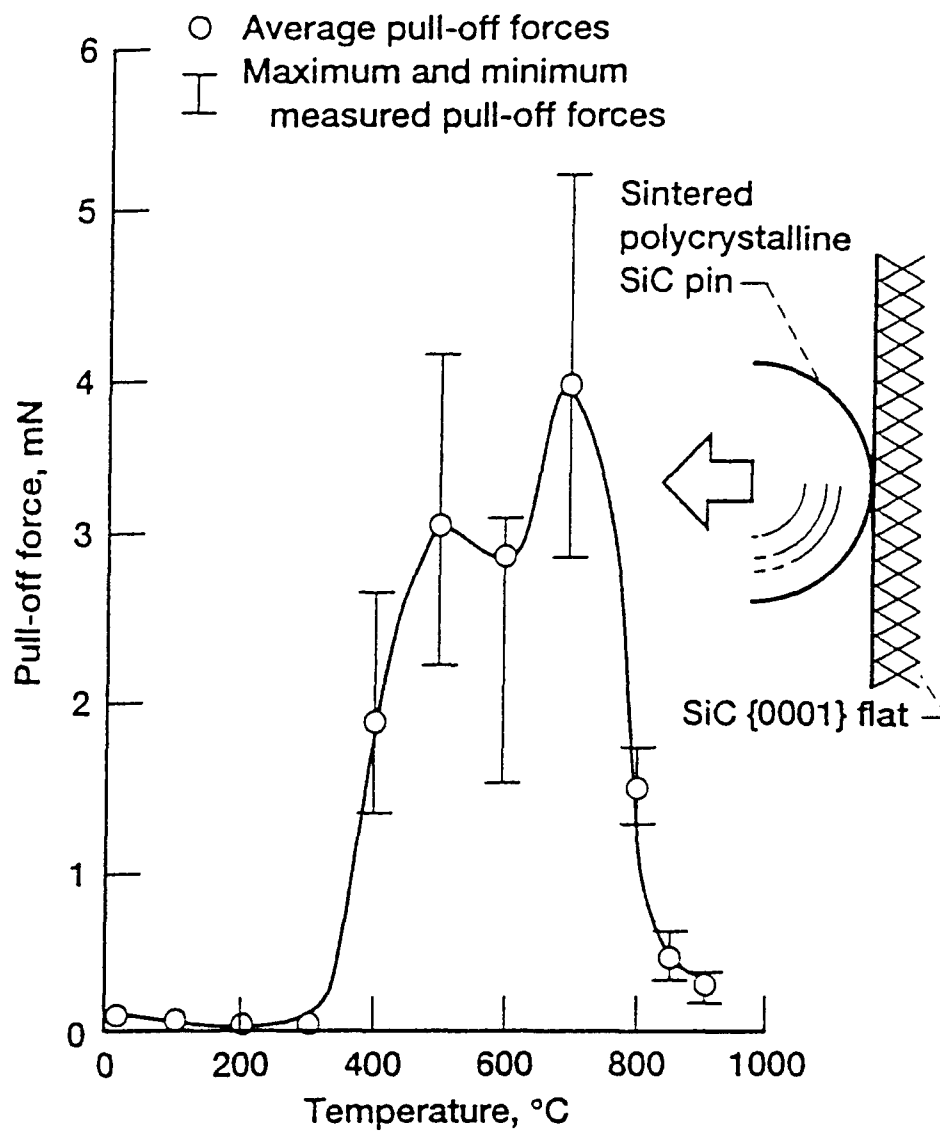


Figure 23. Pull-off force (adhesion) as a function of temperature for SiC {0001} flat surfaces in contact with sintered polycrystalline SiC pins in ultrahigh vacuum; from [4].



Figure 24. Shallow angle SEM photo of the $\sim 2\text{ }\mu\text{m}$ -thick UNCD-coated CERCOM SiC-B tribopin positioned in its graphite fixture, right after removal from the deposition chamber.

Unpolished-UNCD-Coated Cercom SiC-B

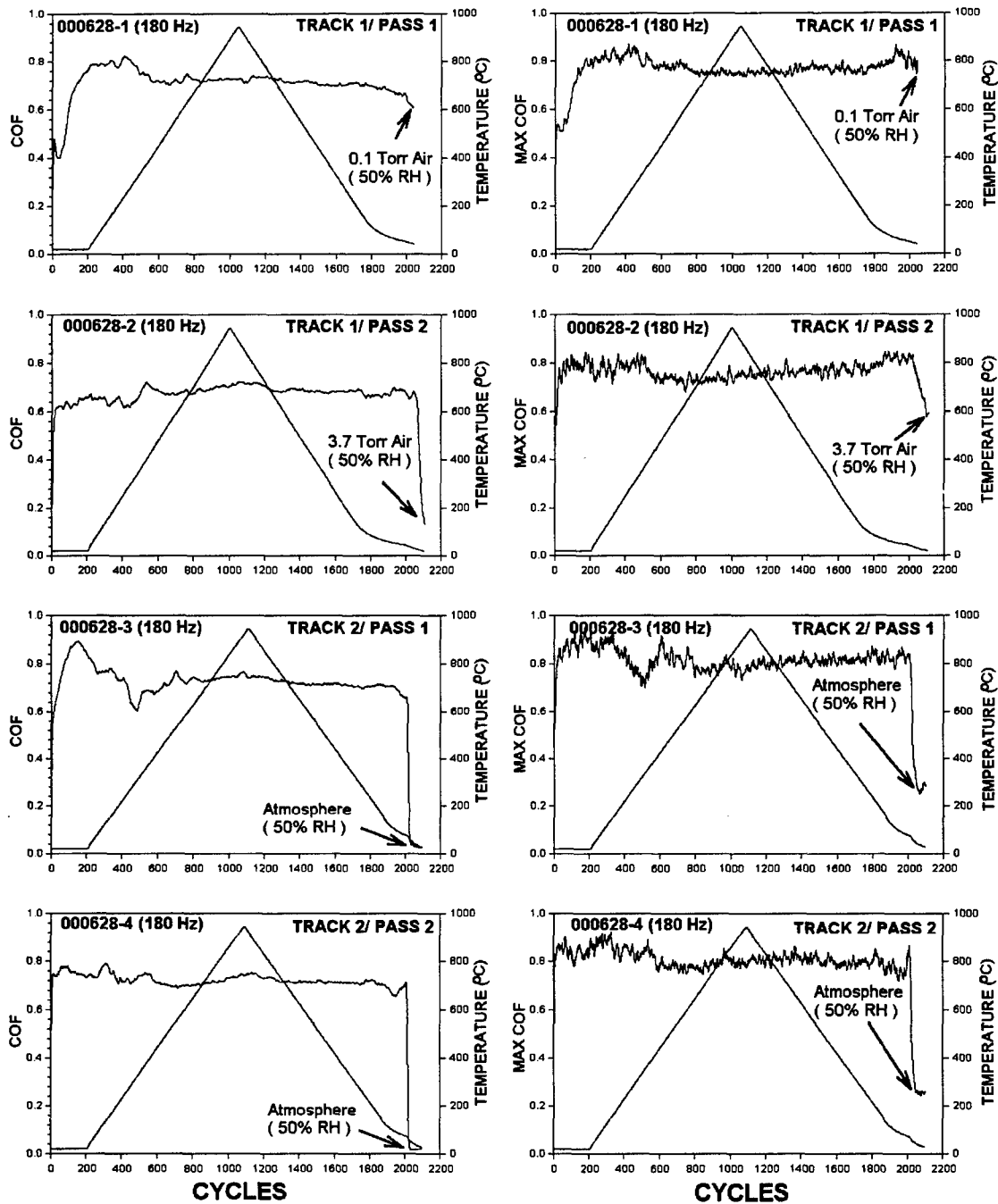


Figure 25. COF and MAX.COF of the UNCD in vacuum. Note graphite-like (high friction) behavior in vacuum, and favorable (equally graphite-like) friction response to various partial pressures of 50% R.H. air admitted into the chamber.

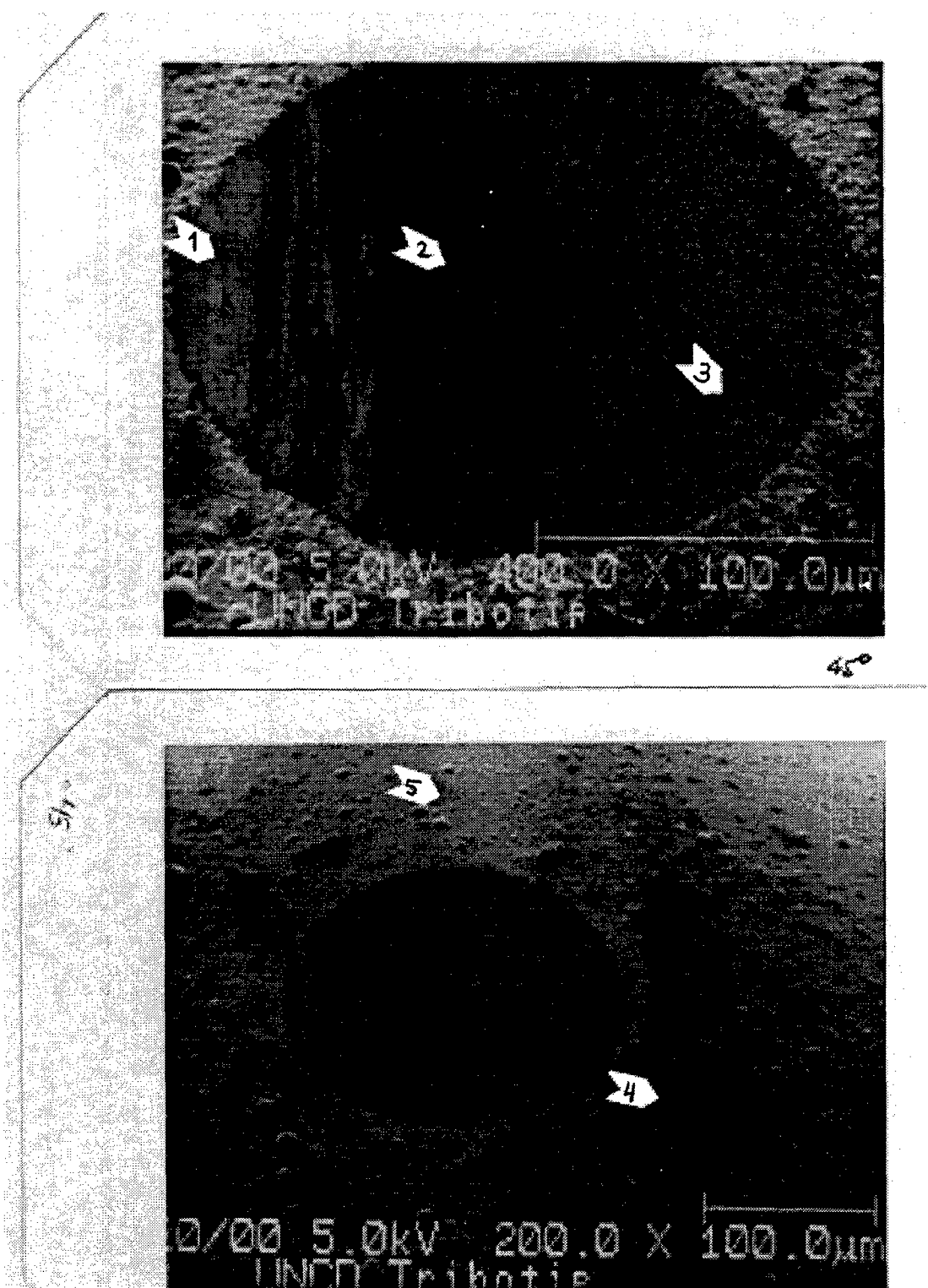


Figure 26. Size and appearance of the worn UNCD on the pin tip scar. Numbers indicate sites of forthcoming AEX/XPS/micro-Raman examinations.

APPENDIX:

**W. Kibbey Stovall, "SiC Tribopin Analysis, Hexoloy
Source" Raytheon ES M&P Dept. Surface Analysis
Laboratory Report, 9/20/00.**

**M & P DEPARTMENT
SURFACE ANALYSIS LABORATORY REPORT**

TO	Mike Gardos	SOURCE CODE	72-50-01	LOC	E0	BLDG	E01	M/S	F150	PHONE	647-4357
FROM	W. Kibbey Stovall	SOURCE CODE	72-53-20	LOC	E0	BLDG	E01	M/S	F150	PHONE	647-4391, -3560
SUBJECT	SiC Tribopin Analysis, Hexoloy Source									DATE	9/20/00

SUMMARY

The submitted tribopins were analyzed by AES and XPS to determine the surface atomic composition of the wear scars and pin tips. Carbon was observed to occur on pin tips in carbidic, graphitic, and partially oxidized states. Silicon was observed in carbidic and partially oxidized states as well. Oxygen was only seen in one binding energy state which was assigned to both carbon and silicon sources.

PROCEDURE

Both Auger Electron Spectroscopy (AES) and X-ray Photoelectron Spectroscopy (XPS or ESCA) were used to characterize the samples. Because the wear scars were less than the smallest aperture size available (200 μm diameter), the XPS spectra taken therefore include information about the pin tip surface outside the scar. For the smaller areas on the wear scar, AES was used. The minimum size for this technique was approximately 10 μm , which was often the size of the regions of interest. Some overlap of surface regions, especially in the high kinetic energy peaks, should therefore be expected for the analyses of the smallest areas.

For the AES work, a 5 keV electron beam was used as the excitation source. For XPS, aluminum X-rays were used. Both techniques depended on a hemispherical mirror analyzer for spectral separation, with the AES method operating in fixed retard ratio mode and with XPS done in fixed analyzer transmission mode. Elemental analyses were performed by integrating peak areas (XPS) or measuring peak to peak separation of the spectral differential (AES) for appropriate electron energy lines, adjusting for sensitivity factors, and normalizing the results.

A 4.0 keV argon ion sputter gun, calibrated to sputter 50 $\text{\AA}/\text{min}$ of Ta_2O_5 , was used to remove material from a 2 mm x 2 mm spot on each sample.

The pins were mounted as close to vertical as possible, this resulted in a 45° image angle for all of the SEM images taken by the instrument. The AES spectra were run with low beam currents (<5 nanoamps) to minimize both beam damage and charging effects.

EXPERIMENTAL RESULTS

The data for each of the tribopins tested is summarized on this and the following three pages, with each page being dedicated to the results and observations for a single pin only. The original spectra and unreduced data are attached along with the corresponding SEM images at the end of the report.

Surface Analysis for Hexane Washed, HF Etched, and Vacuum Tested Tribopin

AES Survey Results: Hexane/HF/Vacuum
Tribopin P/N 980302-1/-4, Hexoloy SiC, Filename 0699SICC#

Location	Depth	Atomic Concentration					File #
		C	N	O	Si	Cl	
Wear Scar, Large Area	Surface	54		15	31		1
"	-5Å	57		22	22		7
Wear Scar, Edge	Surface	62		18	20		3
"	-5Å	53		24	23		9
Wear Scar, Center	Surface	64		18	18		4
"	-5Å	58		18	23		10
Wear Debris	Surface	66	2	10	22	1	2
Tip, Off-Scar	Surface	61		11	27		5
"	-5Å	58		4	38		11

XPS Survey Results: Hexane/HF/Vacuum
Tribopin P/N 980302-1/-4, Hexoloy SiC, Filename 0699SICC#

Location	Depth	Atomic Concentration					File #
		C	N	O	Si		
Whole Tip	-5Å	52		16	32		8

XPS Multiplex Results: Hexane/HF/Vacuum
Tribopin P/N 980302-1/-4, Hexoloy SiC, Filename 0699SICC6

Location	Depth	High Resolution Spectral Data		
		C	O	Si
Whole Tip (includes Scar, Debris, and Unworn areas)	-5 Å	55 at%	15 at%	30 at%
		283.7 eV: 92.5%	532.0 eV: 100.0%	100.1 eV: 75.3%
		286.2 eV: 7.5%		102.2 eV: 24.7%

Observations

Surfaces were very poorly conductive before sputtering, usually producing significant spectral shifts in AES, even when running with minimal beam currents (<2 nanoamps). Also, the SEM images show the wear scar to look more roughened than polished by the testing.

Surface Analysis for Hexane Washed, HF Etched, and 0.2 Torr O₂ Tested

Tribopin

AES Survey Results: Hexane/HF/0.2 Torr O₂

Tribopin P/N 980303-1/-4, Hexoloy SiC, Filename 0699SICB#

Location	Depth	Atomic Concentration				File #
		C	O	Si		
Wear Scar, Smooth Area	Surface	100				3
"	-5Å	82	4	14		5
Wear Scar, Rough Area	Surface	100				4
"	-5Å	94	6			6
"	-10 Å	98	2			7
Wear Scar, Large Area	-10Å	100				9
Wear Debris	Surface	62	19	19		1
Tip, Off-Scar	Surface	70	10	20		2
"	-10Å	54	14	33		8

XPS Survey Results: Hexane/HF/0.2 Torr O₂

Tribopin P/N 980303-1/-4, Hexoloy SiC, Filename 0699SICB#

Location	Depth	Atomic Concentration				File #
		C	O	Na	Si	
Whole Tip	-10Å	63	14	1	23	10

XPS Multiplex Results: Hexane/HF/0.2 Torr O₂

Tribopin P/N 980303-1/-4, Hexoloy SiC, Filename 0699SICB11

Location	Depth	High Resolution Spectral Data		
		C	O	Si
Whole Tip (includes Scar, Debris, and Unworn areas)	-10 Å	68 at%	14 at%	19 at%
		283.5 eV: 29.4%	531.9 eV: 100.0%	100.3 eV: 71.3%
		284.4 eV: 63.6%		102.1 eV: 28.7%
		287.0 eV: 7.0%		

Observations

The bright and dark contrasted areas seen in the high resolution SEM images were not seen here. The near absence of silicon from the wear scar surface is real. Even though the smooth area at -5Å depth numerically produces a value of 14 at% for silicon, this value is at the noise level in the spectrum.

Surface Analysis for Hexane Washed, HF Etched, and 3.4 Torr O₂ Tested Tribopin

AES Survey Results: Hexane/HF/3.4 Torr O₂

Tribopin P/N 990104-1/-4, Hexoloy SiC, Filename 0699SICA#

Location	Depth	Atomic Concentration					File #
		C	O	Si	N	S	
Wear Scar, Low Relief #1	Surface	57	8	35			2
Wear Scar, Low Relief #2	Surface	64	6	29			3
Wear Scar, Low Relief	-5A	54	10	35			5
Wear Scar, High Relief	-5A	42	30	28			6
Wear Debris	Surface	45	28	26			1
"	-5A	31	43	26			7
Wear Debris, Fiber Rich	-5A	56	16	26	2	<1	8
Tip, Off-Scar	-5A	49	13	37		<1	9

XPS Survey Results: Hexane/HF/3.4 Torr O₂

Tribopin P/N 990104-1/-4, Hexoloy SiC, Filename 0699SICA#

Location	Depth	Atomic Concentration					File #
		C	N	O	Na	Si	
Whole Tip	Surface	46	1	27	<1	25	4
"	-5A	44		27		29	11

XPS Multiplex Results: Hexane/HF/3.4 Torr O₂

Tribopin P/N 990104-1/-4, Hexoloy SiC, Filename 0699SICA10

Location	Depth	High Resolution Spectral Data		
		C	O	Si
Whole Tip (includes Scar, Debris, and Unworn areas)	-5A	43 at%	28 at%	28 at%
		283.7 eV: 76.0%	532.2 eV: 24.8%	100.1 eV: 54.4%
		287.0 eV: 24.0%	535.2 eV: 75.2%	102.5 eV: 11.5%
				105.8 eV: 34.1%

DISCUSSION

Quantitative Analysis

Using AES for precise compositional analyses is always problematic. The emissions of Auger electrons have to be differentiated from the large secondary electron background and thus a significant amount of beam current must be used to obtain a useful signal to noise ratio. However, increasing the beam current also causes surface damage and localized chemistry (typically carburization and oxidation) during the analysis, especially for insulating surfaces. For all the AES spectra taken for this study, the beam current was limited to less than 5 nanoamps as a compromise value. Even then, there was visible beam damage after all acquisitions. This beam-induced damage was thin, as 5 Å of sputtering would remove it. So when reviewing the quantitative AES data, it should be assumed that some of the measured carbon and oxygen are from this source and not the actual surface.

The tribotips from the vacuum and 0.2 torr oxygen tests did not show any significant variation in composition across the surfaces of their wear scars. The 3.4 torr oxygen test did show a pronounced oxygen enhancement on the high relief surfaces versus the lower areas in its wear scar. In these areas of higher oxygen content both the Si:O and C:O ratios drop approximately 75% relative to the low relief areas (when comparing sputtered surfaces).

It is difficult to find trends between these three samples. There was a clear difference in surface composition between the 0.2 torr tested pin and the other two pins. The 0.2 torr tested pin showed the least surface oxygen and silicon in its wear scar of any sample, to the extent that silicon was only tentatively assigned at the noise level after sputtering in one spectrum! In contrast, both the vacuum tested and 3.4 torr tested pins showed surface oxygen in their wear scars, with the vacuum tested having an average value of 21 at% and the 3.4 torr tested showing 10 at% on low relief 30 at% on high relief areas.

The trends seen that do correlate with the oxygen partial pressure during the tribotesting are for the wear debris and the unworn surface composition. The fine granular wear debris, which was present in all three samples, did increase in oxygen content with increasing oxygen pressure. The trend for unworn surface chemistry was not as pronounced, but it does appear that the vacuum test produced the least oxidation of the surrounding tip surface, as its oxygen content falls to less than 5 at% with only 5 Å of sputtering.

Qualitative Analysis

Normally, XPS does not suffer the same problems of interpretation that AES does. In this case, however, because the wear scar and its features were smaller than the smallest XPS aperture available (200 microns), a new set of problems were encountered. None of

the wear scars showed a homogeneous surface. Furthermore, since the XPS surveys and multiplexes were taken with a 200 micron aperture, the resulting spectra also include unworn areas and wear debris on the tips surrounding the wear scars. Thus, the XPS spectra represent area-weighted averages of the various surfaces exposed within a 100 micron radius of the center of each wear scar.

High-resolution XPS spectra are used to show the chemical states of elements. In this case, the chemical states are assigned by correlating the peak energies of the deconvoluted C 1s, O 1s, and Si 2p emissions with reported energies from known samples. As before, the spatial limitations of XPS cause some unworn area on the tips to be included in the spectra, as well as some wear debris. This precludes using the integrated areas of the deconvoluted peaks as measures of wear scar chemical composition, since the area-weighting factors are not known. However, the peak location values are still meaningful, as they represent the majority states of the elements on the wear scars and surrounding tip surfaces. Thus, qualitative analysis is possible even though quantitative analysis is not.

In the case of carbon's 1s emission, the XPS multiplexes for the three samples show the element to be in three binding energy states, averaging 283.6 eV, 284.4 eV, and 286.7 eV. The lowest value best corresponds with reference values for carbidic carbon (280.7 – 283 eV) and occurred for all pins. The middle value is in the range of graphitic (284.2 – 285.0 eV) carbon, and only strongly appeared in the 0.2 torr tested sample. The high energy value was seen in all three pins and best matches with the expected energies of carbon atoms singly or doubly bonded to oxygen (286.0 – 288.0 eV). This would include alcohol, ether, ketone, and aldehyde functionalities, but exclude carboxyls and carbonates.

The Si2p emissions showed two dominant components, a low energy peak at 100.1 eV and a higher peak at 102.3 eV, and an aberrant 105.8 eV peak for the 3.4 torr tested pin. The low energy peak falls at the low end of the reported values for carbides (99.9-100.9 eV), while the higher peak overlaps best with silicates (102.0-103.0 eV). The reported range for silicon dioxide does not begin until binding energies in excess of 103.2 eV are reached, but no reported silicon valence is in excess of 104.5 eV.

The oxygen 1s emissions occurred only as single peaks for the vacuum and 0.2 torr tests, but the 3.4 torr test also gave a majority component at higher energy. The low energy peaks were centered around 532.0 eV, which is lower than the values typically reported for SiO₂ (532.5-534.3 eV), but is similar to values seen for organic carbonyls such as *p*-benzoquinone and benzamide. The high energy peak seen for the 3.4 torr tested pin appeared at 535.2 eV, above the reported valence of any oxygen species.

When interpreting the photoelectron data it should be remembered that they represent the area-weighted averages of the whole tip surfaces, which included the wear scar, wear debris, and unworn tips. Furthermore, peak fitting is more art than science and an effort was made only to use the minimum number of peaks required to produce a good mathematical fit for the data. However, because it was felt that for the 0.2 torr carbon 1s

test data this did not produce realistic results, an additional peak was used to produce values more in line with previous interpretations. Having said all that, the vacuum tested pin seems most consistent with its experimental conditions. Its surface showed primarily carbidic carbon with a lesser amount of oxygenated carbon, it showed carbidic silicon and oxygenated silicon, and it showed a single oxygen value appropriate to both. The valences seen on the 3.4 torr tested pin were essentially the same as for the vacuum tested pin, with the additional anomalous high valence oxygen and silicon peaks attributed to localized regions of silica which charged slightly and therefore shifted their peaks. These regions are most likely in the wear debris, judging by the high O:Si ratio seen there by AES. The 0.2 torr tested pin's elemental analyses and photoelectron results suggested that its surface carbon was primarily graphitic with smaller amounts of carbidic and oxygenated carbon, its silicon was both carbidic and oxygenated, and its oxygen value appropriate to both.

The careful reader will notice there was no graphitic carbon 1s content assigned to the vacuum and 3.4 torr tested pins, but this only means sufficiently good fits to the data were obtained using just the carbidic and oxygenated peaks. It is certainly possible to add a graphitic peak and obtain a good fit, but the contribution to the overall peak shape from this valence would be small.

CONCLUSIONS

This report does not intend to make any statements about the mechanisms of surface wear and reconstruction related to the pins tested herein, but the very different surface chemistry of the 0.2 torr tested pin relative to the remaining samples suggests a very different mechanism of wear must have been operating under those conditions. What appears to be a near complete graphitization of the wear scar stands apart from the mixed carbon/oxygen/silicon surfaces seen on the other pins. The increasing oxygen content of the wear debris seen across all the pins, and the increasing oxygen content of the wear surfaces (high relief) might also be expected from increasing the oxygen pressure during the tests.

Kibbey Stovall